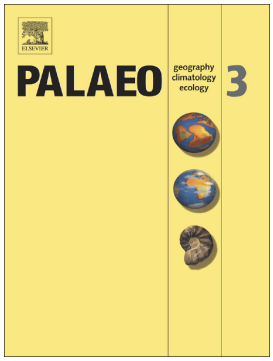

Volcanism, redox conditions, and microbialite growth linked with the end-Permian mass extinction: Evidence from the Xiajiacao section (western Hubei Province), South China

Yu Pei, Zhong-Qiang Chen, Yuheng Fang, Stephen Kershaw, Siqi Wu, Mao Luo

PII: S0031-0182(17)30487-X
DOI: doi: 10.1016/j.palaeo.2017.07.020
Reference: PALAEO 8370

To appear in: *Palaeogeography, Palaeoclimatology, Palaeoecology*

Received date: 7 May 2017
Revised date: 16 July 2017
Accepted date: 18 July 2017

Please cite this article as: Yu Pei, Zhong-Qiang Chen, Yuheng Fang, Stephen Kershaw, Siqi Wu, Mao Luo , Volcanism, redox conditions, and microbialite growth linked with the end-Permian mass extinction: Evidence from the Xiajiacao section (western Hubei Province), South China, *Palaeogeography, Palaeoclimatology, Palaeoecology* (2017), doi: 10.1016/j.palaeo.2017.07.020

Volcanism, redox conditions, and microbialite growth linked with the end-Permian mass extinction: Evidence from the Xiajiacao section (western Hubei Province), South China

Yu Pei[a], Zhong-Qiang Chen[a,] *, Yuheng Fang[a], Stephen Kershaw[b], Siqi Wu[a], Mao Luo[c]

[a]*State Key Laboratory of Biogeology and Environmental Geology and School of Earth Science, China University of Geosciences, Wuhan 430074, China*

[b]*Department of Life Sciences, Brunel University, Uxbridge UB8 3PH, UK*

[c]*School of Life and Environmental Sciences, Deakin University, Melbourne Burwood Campus, Victoria 3125, Australia*

*Corresponding author. E-mail address: zhong.qiang.chen@cug.edu.cn (Z.Q. Chen)

ABSTRACT

A new Permian–Triassic boundary microbialite (PTBM) is described from the Xiajiacao section of western Hubei Province, South China. The new microbialite, 3.16 m thick, comprises a thin layer of stromatolite and a thick thrombolite unit. An irregular contact separates the uppermost Permian skeletal packstone from the post-extinction stromatolite, but it is not yet possible to discriminate whether it was formed by submarine solution in the wake of ocean acidification or subaerial exposure due to regional regression, or a combination of both. The stromatolite shows “cabbage-like” morphology, and the thrombolite is characterized by centimetric clotted texture. Abundant columns of the microproblematica structure *Gakhumella*, coccoid-like spheroids, clumped spheroids, and hollow spheroids are recognized in both

stromatolites and thrombolites and may have played an important role in accretion of the microbialites. Pyrite framboid analysis indicates that microbialites may have been affected by lower dysoxic to upper dysoxic conditions in the immediate aftermath of the Permian–Triassic extinction. Stratigraphic abundance of both high-temperature grains (β-quartz and glassy balls) peaked ~20 cm below the biotic extinction horizon, implying that either intensive volcanic eruption occurred only just prior to biotic extinction, or volcanism was still intensive during biotic extinction, but volcanic grains were not deposited in the Xiajiacao locality, likely due to the shallow, agitated environment caused by the regional regression. Overall, microbial bloom, indicated by the widespread PTBMs, seems to have been little affected by the contemporaneous volcanism.

Keywords: stromatolite; thrombolite; microbial bloom; Permian–Triassic boundary; felsic volcanism; framboidal pyrite

1. Introduction

The Permian–Triassic (P–Tr) mass extinction is the severest ecological catastrophe during the Phanerozoic, and it resulted in not only biodiversity decline but also stimulated the widespread deposition of unusual biosedimentary structures during this critical period (Chen and Benton, 2012). In particular, the pronounced P–Tr boundary microbialite (PTBM) deposits were widespread in shallow platform settings in low latitude regions, especially South China, Vietnam, Saudi Arabia, Turkey, Iran, and Hungary in the Paleo-Tethys, and some Panthalassic seamounts embedded in the accretionary complexes of Japan (Lehrmann, 1999; Kershaw et al., 1999, 2002, 2007, 2012; Ezaki et al., 2003, 2008; Wang et al., 2005, 2016; Liu et al., 2007; Yang et al., 2008, 2011; Wu et al., 2014, 2017; Lehrmann et al., 2015; Zheng et al., 2016; Adachi et al., 2017; Fang et al., 2017a; Tang et al., 2017). These PTBMs are believed to indicate microbial bloom and may represent a harsh environment linked with the end-Permian crisis (Bottjer et al., 2008; Chen and Benton, 2012). However, recent studies on the PTBMs showed that plentiful infaunal metazoans dwelled in microbialites (Liu et al., 2010; Yang et al., 2011, 2015a, b; Forel et al., 2009; 2012; Forel, 2013). The ostracod assemblage indicates that microbialites may be formed in a well-oxygenated habitat (Liu et al., 2010; Forel et al., 2009). Thus, the paleoenvironmental settings, particularly redox condition, of the PTBMs require careful interpretation. Although most Triassic microbialites are believed to be biogenic, very few examples (but see Chen et al., 2014) have proved the possible constructing micro-organisms of these microbial carbonates. The PTBMs therefore remain enigmatic in terms of geobiologic accretion process and biogenicity (Kershaw et al., 2012).

Moreover, the widely recognized irregular contact surface between the microbialite and underlying bioclastic limestone has attracted increasing interest from global sedimentologists and paleontologists. It still remains an open question whether this irregular contact resulted from submarine solution in the wake of ocean acidification or subaerial exposure due to regional regression (Payne et al., 2007; Liu et al., 2007; Collin et al., 2009; Wignall et al., 2009; Yin et al., 2014; Jiang et al., 2014; Lehrmann et al., 2015, 2016; Kershaw et al., 2016), or a combination of both processes.

Another intriguing question is the relationship between active volcanism and contemporaneous microbial blooms during the P–Tr transition. Biomarker analysis suggested that the P–Tr microbial blooms may have been triggered by extensive volcanism during that time (Xie et al., 2010). Recently, Fang et al. (2017b) also detected abundant annular, granular, and tubular bioalteration textures, which are interpreted as the products of microbial dissolution of volcanic glass. Fossilized organic remains (e.g., small coccoid-like spheroids, rods, filaments, and thin-films) are identical to extracellular polymeric substances of microorganisms. Microbial blooms in the P–Tr boundary ash layers may attest to the severity of environmental stresses that prevailed during this crisis (Fang et al., 2017a). Since the PTBMs have been widely accepted as indication of microbial proliferation (Kershaw et al., 2012; Chen and Benton, 2012), the PTBM sections provide unique opportunities to test the causal link between volcanism and microbial proliferation over the P–Tr transition.

Here we describe and interpret a newly discovered PTBM with a pronounced irregular contact beneath its base in the Xiajiacao section of Lichuan area, western Hubei Province, South China (Fig. 1A). This study aims to assess the processes of formation, including the redox condition, of this new PTBM by means of detailing

petrologic features, microfacies analysis, and pyrite framboid analysis. The causal link between volcanism and microbial bloom in the aftermath of the P–Tr mass extinction is also tested based on a count of high-temperature quartz and glass grains, derived from felsic volcanism (Yang et al., 1991; Gao et al., 2013) throughout the studied section.

2. Geological and stratigraphic settings

The studied section is located at the Xiajiacao, ~20 km west of Wangying Town, Lichuan City, western Hubei Province, South China (Fig. 1A), and was situated on the northern margin of the Yangtze Platform during the P–Tr transition (Feng et al., 1997; Fig. 1B). The lower part of the section comprises massive skeletal packstone of the Changxing Formation (Fig. 2). The overlying Daye Formation, composed mainly of thick-bedded microbialite, thin-bedded wackestone, and mudstone, crops out in the upper part of the studied section (Fig. 2). The onset of microbialite is marked by a distinct irregular contact surface, separating from the underlying skeletal packstone. Recently, Yu et al. (2015) found conodont *Hindeodus parvus* from the upper part of the microbialite, although this index species often first occurs in the lower part of the PTBMs (Yang et al., 2011; Kershaw et al., 2012) or the base of the PTBMs (Jiang et al., 2014; Wang et al., 2016) elsewhere in South China. Abundant foraminifera recognized from the uppermost Changxing Formation are assignable to the *Palaeofusulina sinensis* Zone, the topmost Changhsingian fusulinid zone in the Meishan section and other areas of South China (Song et al., 2009; Chen et al., 2015). In addition, carbonate carbon isotopes show a distinct negative shift from 2.21‰ at Bed 1 to 1.66‰ at Bed 2 (Yu et al., 2015), marking the end-Permian mass extinction,

as recorded in other PTBM sections in South China (Krull et al., 2004; Mu et al., 2009; Yang et al., 2011; Wu et al., 2017). Accordingly, the end-Permian mass extinction is calibrated to the base of Bed 2, and the P–Tr boundary is tentatively placed at the upper part of Bed 6 (Fig. 2).

3. Methods

Five polished slabs and 59 petrographic thin sections were petrologically analyzed to shed light on the genesis of the Xiajiacao microbialite. Freshly broken rock samples were washed using water and rinsed for approximately 10 seconds in 10% acetic acid and observed to detect potential microbes under a HITACHI-SU8010 Field Emission Scanning Electron Microscope (FESEM) at the State Key Laboratory of Biogeology and Environmental Geology, China University of Geosciences (Wuhan), China. Element mapping of energy dispersive X-ray spectrometry (EDS) analysis was also employed to indicate the relative contents and distributions of various elements in microbialite. Size and morphologic analyses of pyrite framboids were also obtained from 11 samples from microbialite, plus another three from the underlying skeletal packstone, and three more from wackestone and mudstone overlying the microbialite (Fig. 2). A polished surface (2×2 cm) of each sample was examined for pyrite framboid analysis using the FESEM. Caution is needed for these small framboids because they may not be completely exposed on surfaces examined (Hethke et al., 2013). Both framboid size and morphology (Bond and Wignall, 2010; Huang et al., 2017), and the cross-plot diagram of mean framboid size versus standard deviation (Wilkin et al., 1996) are applied to interpret redox conditions during the development of microbialite. It is important to clarify that pyrite framboids form in

anoxic conditions in the redox boundary, but the diameters of framboids have been shown to reflect the state of oxygenation of the water above the location of their formation in modern environments (e.g. Bond and Wignall, 2010; Wilkin et al., 1996). Thus, in places where framboids have mean diameters of 6–10 μm and are moderately common, with a few, larger framboids together with some crystalline pyrite, they could indicate weakly oxygenated bottom waters above the locations of formation of the framboids. In the anoxic sediments below water that has upper dysoxic conditions (with partial oxygen restriction in bottom waters), framboids are commonly to rarely present, with a broad range of sizes, only a small proportion of framboids <5 μm, and the majority of pyrite crystals (Bond and Wignall, 2010; Huang et al., 2017). Also, quartz crystals and volcanic glass material were extracted from 30 samples and their occurrence abundance in per sample of 0.5 kg was also counted in order to estimate volcanic eruption intensity.

4. Results

In outcrop, the microbialite, 3.16 m thick (Fig. 3A), comprises a thin layer of stromatolite (8 cm thick) (Fig. 3B–D) followed by thin-bedded finely crystallized dolomitic limestone (8 cm thick) (Fig. 3B) and thick-bedded thrombolite (3 m thick) (Fig. 3E). The Permian skeletal packstone (Fig. 4A) underlies the stromatolite (Fig. 3B–D). The dolomitic micrite (Figs. 3B, 4B) and thrombolite (Figs. 3E, 4C–F) are overlain by wackestone and mudstone.

4.1. Non-microbialite facies

The uppermost Permian skeletal packstone (Bed 1 in Fig. 2) comprises allochem assemblage of foraminifers, including *Colaniella*, *Ichthyofrondina*, and *Palaeofusulina*, macro-algae, echinoderms, gastropods, brachiopods, bivalves, and ostracods (Fig. 4A). Compared with the lower part, the uppermost part of the skeletal packstone, separated from overlying strata by an irregular interface (Fig. 5), may be formed in a higher energy environment (Fig. 2), with the common occurrence of truncated skeletons or tests and geopetal structures (Fig. 5A, C–D, G). The environment changed from upper subtidal zone below fair-weather wave action in the lower and middle parts of the latest Permian skeletal packstone to the intertidal zone of the uppermost part of the skeletal packstone unit (Fig. 2).

The thin layer of stromatolite (Bed 2 in Fig. 2) overlies skeletal packstone with a distinct irregular contact surface between the two. Above the stromatolite, dolomitization has seriously affected the limestone (Bed 3 in Fig. 2), forming wedge-shaped finely crystalline dolomitic limestone (Figs. 3B, 4B). Thin-bedded wackestone (Bed 7 in Fig. 2) caps the thrombolite unit (Bed 6 in Fig. 2), with similar lithology also occurring in Bed 9 (Fig. 2). Overlying the wackestone bed (Bed 7 in Fig. 2), thin-bedded mudstone (Bed 8 in Fig. 2) is conspicuous in the field. Thin-bedded wackestone intercalated with mudstone may represent a low energy environment, maybe deep subtidal zone below fair-weather wave action zone (Fig. 2).

4.2. Irregular contact between microbialite and bioclastic limestone

An evident irregular surface characterizes the contact between the latest Permian skeletal packstone and the earliest Triassic stromatolite (Figs. 3B–D, 5). Skeletal packstone mingles with overlying stromatolite or deposits of inter-stromatolites (Fig.

5B). Along the interface, some organism bodies were truncated. For instance, algal skeletons and foraminiferal tests in the Permian skeletal packstone are clearly truncated, with irregular, sharp contacts (Fig. 5C–D). Others existed along the surface but were not truncated (Fig. 5E). Syntaxial cement possibly on crinoid fragments is also commonly present in skeletal packstone near the irregular contact (Fig. 5F). Geopetal structures are found among bioclasts in the Permian skeletal packstone (Fig. 5A, G). Precipitation of two generations of intergranular, finely crystalline, anisopachous marine cements is around grains (Fig. 5G–I). The thickness of cements is highly variable (Fig. 5H–I). It ranges from 10 μm to 40 μm. When the anisopachous cement is thicker around the lower parts of grains, pendent cements (Fig. 5A) are pronounced, in topmost skeletal packstone, as recognized by Collin et al. (2009) and Wignall et al. (2009) from the contemporaneous skeletal packstones elsewhere in South China. Etched grains, pendent cements, anisopachous cements and geopetal sediments may be interpreted as vadose, under conditions of sub-aerial exposure (Collin et al., 2009).

4.3. Geobiologic accretion of microbialites

4.3.1 Macroscopic features of stromatolite and thrombolite

The stromatolite shows “cabbage-like” morphology, featured by crinkled, wavy laminae on vertical profile (Fig. 3B–D). Stromatolitic columns are usually 2–3 cm in diameter and 6–8 cm in height. Characterized by centimetric clotted textures, the overlying thrombolite consists of distinct micritic and sparry calcite when viewed on polished slabs. Micritic masses are of relatively light color, while coarser ones exhibit

darker patches without orientation (Fig. 3E). The thrombolite can be divided into three parts based on the relative amount of micritic and sparry calcite. The middle part has relatively lower content of micrite (Fig. 2).

4.3.2 Microscopic features of microbialite

The thrombolite comprise irregular sparitic masses (light-colored areas) and micritic clots (dark-colored areas) (Fig. 4C), corresponding to dark-colored, coarsely crystallized masses and light-colored micritic masses in polished blocks, respectively (Fig. 3E). Sparitic masses are composed of coarsely crystalline calcite, while micritic masses are made of finely crystalline calcite, forming a mosaic pattern. In micritic calcite, metazoans, such as ostracods, gastropods, and microconchids are present, especially in the middle part of the thrombolite (Fig. 4D–F).

Columnar objects and various spheroids of potential microbes are abundant. The former are common in stromatolite and thrombolite (Fig. 6). They can exist separately (Fig. 6A–F) or as aggregates (Fig. 6G–I). Single columns are straight (Fig. 6A–C) or slightly incurved (Fig. 6D–E). Small rounded spheroids are commonly present in both stromatolite and thrombolite. As a whole, two types of spheroids are observed. Type-1 are characterized by a sparitic calcite nucleus surrounded by micritic sheaths, 50-100 micron in diameter (Fig. 7A–G). Type-2 consist of micritic calcite nuclei coated with sparitic calcite sheaths, 50-80 micron in diameter (Fig. 7H–I), identical to bacterial clump-like spheroids (BCSs) (Luo et al., 2016; Fang et al., 2017a).

4.3.3 Ultrastructure of microbialite (SEM features)

Both columnar objects and spheroids are also observed under SEM. Each single column has a large, rounded proto-chamber followed by a series of thin segments arching in the same direction (Fig. 8). Each individual possesses 10–30 distinct segments with a thin but distinct chamber between two segments. Each chamber is ~2 μm thick, and filled with microsparitic calcite.

Spherical objects can be categorized into three types: type-1) coarse sparry nucleus coated with radiating rays (Fig. 9A); type-2) a rounded nucleus that comprises radiating rays surrounded by coarse radial rays (sparitic sheaths) (Fig. 9B–E). The round nucleus is also covered by one thin micritic layer, which is pronounced in well-preserved examples (Fig. 9B), but disappears in poorly preserved examples (Fig. 9C–E); type-3) a void nucleus coated with radiating rays (Fig. 9F–H).

4.4. Pyrite framboid analysis

A total of 946 pyrite framboids from 11 samples of microbialite were measured. No framboids were found in all skeletal packstone samples, and among the three samples from wackestone and mudstone beds capping the microbialite, only one sample yielded abundant framboids. Pyrite framboids may clump together or scatter separately (Fig. 10A–D). “Box-and-whisker” plots show the varied patterns of framboidal size distributions throughout the section. Framboids embedded within stromatolite layer show a mean diameter of 9.87 μm, reduce to 6.30 μm in diameter in overlying dolomitic limestone (Bed 3), then increase in size to 9.30 μm in diameter throughout most parts of Bed 4, with a slight size reduction at the top of this bed. The framboid sizes increase in Bed 5, reaching the maximum value of 12.07 μm in mean diameter, then decline all the way to the upper portion of the microbialite (9.05 μm in

mean diameter) (Bed 6). The majority (78.6%) of all framboids embedded in microbialite are larger than 6 μm and the mean diameter is 9.43 μm, commonly interpreted as indicating a lower-upper dysoxic environment (Bond and Wignall, 2010; Huang et al., 2017) (Fig. 11), discussed later. Wackestone (Bed 8) above the microbialite yields very small framboids with a mean diameter of 5.76 μm (Fig. 2), indicating a possible anoxic condition in the water above the sea floor where these framboids were deposited (Bond and Wignall, 2010).

4.5. Felsic volcanism products

Both high-temperature quartz crystals and volcanic glass are commonly present in the P–Tr successions in South China, pointing to a felsic volcanism in origin (Yang et al., 1991). Abundant bipyramid-shaped quartz crystals and glassy balls are also abundant in the Xiajiacao section and range from 150 to 250 μm in diameter (Fig. 10E–I). Smaller quartz grains are scattered loosely on surfaces of larger ones (Fig. 10E). Some tiny solid objects have inflated surfaces that are strongly eroded or melted (Fig. 10G), and EDS analysis suggests that they have high contents of Si and O, and thus are actually quartz grains (Fig. 10 L–M). In addition, calcium phosphate is also present in the Xiajiacao samples (Fig. 10J–K, N–O). All features agree well with quartz and glassy balls that are commonly present in felsic volcanic ash beds near the P–Tr boundary in South China (Gao et al., 2013, 2015).

Occurrence abundance (number of grains) of volcanic grains remains at moderate level in the uppermost Permian skeletal packstone (Bed 1), reaches a pronounced peak at the horizon 20 cm below the top of this bed (>100 grains per 0.5 gram sample), then falls rapidly near the irregular contact. The same proxy gently

declines throughout the microbialite to capping wackestone (Beds 2–8), although one moderate surge occurs at the middle part of Bed 4 (Fig. 2).

5.Discussion

5.1. Origin of irregular contact between microbialite and skeletal packstone

A conspicuous irregular surface is beneath the microbialite in Xiajiacao (Figs 3, 5), as observed in other PTBMs elsewhere in South China (Ezaki et al., 2003; Liu et al., 2007; Payne et al., 2007, 2009; Collin et al., 2009; Wignall et al., 2009; Kershaw et al., 2012; Lehrmann et al., 2015).

On one hand, this sharp contact was interpreted as a submarine dissolution surface due to ocean acidification in association with the end-Permian mass extinction in South China(Payne et al., 2007; Lehrmann et al., 2015), which is also interpreted to be equivalent to the hardgrounds of mid-Bed 27 in the GSSP Meishan (Payne et al., 2007). Features supporting ocean acidification include: 1) a lack of exposure characteristics of highstand system tract or sequence development below the truncation surface; 2) absence of boring into the truncation surface; 3) occurrence of a negative carbon isotope excursion above the truncation surface; and 4) complete conodont zones. The dissolution hypothesis is strengthened by the possible acidification indicated by calcium isotopes of whole rocks and conodonts near the P–Tr boundary (Payne et al., 2010; Hinojosa et al., 2010). Modelling of processes affecting the Earth surface during the P–Tr ‘Great Dying’ also strongly supports the occurrence of ocean acidification in that time (Cui et al., 2013).

On the other hand, the possible existence of acidification at the mid-Bed 27 in

Meishan was denied by Chen et al. (2015) who detected complex burrowing systems of *Glossifungites* ichnofacies from Bed 27c in the same section. The largest oceanic acidification indicated by boron isotopic excursions (Clarkson et al., 2015) can be calibrated precisely to the *Isarcicella staeschei* Zone to *I.isarcica* Zone interval, which correlates with the capping carbonates of most PTBMs in South China (Yang et al., 2011; Kershaw et al., 2012; Kershaw, 2016) and thus at a higher level than the extinction horizon. Moreover, Collin et al. (2009) and Wignall et al. (2009) documented vadose evidence showing sub-aerial physical erosion, including geopetal sediments, etched grains, pendent and meniscus cements from the P–Tr boundary beds in the PTMB sections in the Great Bank of Guizhou, southwestern China.

In Xiajiacao, the truncated bioclastic skeletons or tests, geopetal structures, and anisopachous and pendent cements are also commonly observed (Fig. 5). They were interpreted as vadose (Collin et al., 2009). A regional regression corresponding to this irregular contact is also indicated by the loss of 2–3 conodont zones in the regional biostratigraphic correlations (Yin et al., 2014; Jiang et al., 2014). Then the break represented by the irregular contact in most PTBM sections in South China may include part of the topmost skeletal packstone (Bed 1) that has been eroded, stromatolite layer (Bed 2), and its capping dolomitic limestone (Bed 3) in Xiajiacao. In particular, the stromatolite layer is only locally present in some PTMBs (e.g, Fang et al., 2017a) and absent in most PTBMs probably due to erosion related to this regional regression (Yang et al., 2011; Kershaw et al., 2012). This irregular surface, perhaps, represents a depositional hiatus corresponding to the stratal interval ranging from conodonts *Clarkina meishanensis* Zone to *Hindeodus changxingensis* Zone or locally *Hindeodus eurypyge* Zone that is widely recognized from the strata between *Clarkina yini* Zone and *Hindeodus parvus* Zone in South China (Yin et al., 2014;

Jiang et al., 2015; Chen et al., 2015).

Thus both submarine solution in the wake of ocean acidification or subaerial exposure due to regional regression possibly contributed to the irregular surface.

5.2. Geobiologic process and features associated with accretion of the microbialite

The most characteristic problematic calcimicrobes in the Xiajiacao microbialite are columnar objects (Figs 6, 8). They are similar to *Gakhumella*, which is assigned to a kind of green alga, and known from the Permian and Jurassic microbial carbonates (Zaninetti, 1978; Hughes, 2010, 2013). Recently, "*Gakhumella*" is also widely found in the PTBMs in South China (Fang et al., 2017a; Wu et al., 2017), and the "*Gakhumella*" columns are interpreted as crucial constructors of, at least, some PTB microbialites due to their common presence (Fang et al., 2017a). Abundant and diverse spheroids are also pronounced in the Xiajiacao microbialite (Figs 7, 9). Of these, coccoid-like spheroids, with sparitic calcite nuclei surrounded by micritic sheaths (Figs. 7A–G, 9A), are very common. Comparable spheroids have been reported from the PTB stromatolites in Chongyang, Hubei Province, and are interpreted as counterparts of endolithic coccoid bacteria (Yang et al., 2011). Coccoidal spheroids have also been widely reported from the Triassic microbialites (Wang et al., 2005; Mastandrea et al., 2006; Perri and Tucker, 2007; Chen et al., 2014; Luo et al., 2014, 2016), they, however, are usually interpreted as dwellers rather than builders of the microbialites due to their small sizes and rare occurrences (Chen et al., 2014).

Bacterial clump-like spheroids (BCSs), characterized by micritic calcite nuclei enveloped with sparitic calcite rays, are also very abundant in the Xiajiacao

microbialite (Fig. 7H–I). Moreover, the spheroids having nuclei of relatively finer radiating rays coated with much coarser sparitic radiating rays under SEM (Fig. 9B–E) probably can also be categorized into BCSs. BCSs were first found in the present-day travertine deposits (Chafetz and Folk, 1984; Chafetz, 1986), and interpreted as the sedimentary products of microbial carbonates. Similar structures have also been observed in some marine peloidal crusts of other ages, and they have been considered to have a biogenic origin (Reitner, 1993; Reitner and Neuweiler, 1995; Tribovillard, 1998; Folkand Chafetz, 2000; Adachi et al., 2004), with emphasis on nucleation of bacteria clumps (Chafetz and Folk, 1984; Chafetz, 1986; Folk and Chafetz, 2000) or cyanobacterial cells (Kazmierczak et al., 1996; Tribovillard, 1998; Adachi et al., 2004).

Similar spheroids are also commonly present in other PTBMs (Fang et al., 2017a; Wu et al., 2017) and late Early Triassic microbialite (Luo et al., 2016) in South China. These microbialite BCSs may therefore share the same origin as their modern counterparts, and both are likely of biogenic genesis.

In contrast, Bosak et al. (2004) obtained similar marine peloids in their laboratory experiments, and found that purely abiotic process can also lead to the formation of such peloids with a submicro-crystalline center commonly surrounded by a well-developed, euhedral rim of sparry, dentate calcite. However, these abiotic peloids possess radial fabrics within the nucleus, which are distinct from the cloudy, micritic texture found in bacterial clump-like peloids. The type-2 spheroids observed under SEM from the Xiajiacao microbialite also embrace radial fabrics within the rounded nucleus that are surrounded by coarse sparitic sheaths. These types therefore may be classified as abiotic spheroids.

Moreover, the Xiajiacao microbialite also yields some uncommon hollow

spheroids (Fig. 9F–H). Similar objects have been reported from the Lower Triassic microbialites in South China, and regarded as coccoid microbes (Ezaki et al., 2003, 2008; Wang et al., 2005; Yang et al., 2011). Ezaki et al. (2012) interpreted these spheroids to be attributed to sulphate-reducing or anoxygenic phototrophic bacteria.

To sum up, abundant columnar objects and spheroids are likely to indicate an almost exclusively bacterial benthic ecosystem. The various microbial colonies co-existed in different layers within microbialite, as those observed in modern examples (Dupraz et al., 2009). Those bioreactions may have controlled biocarbonate precipitation and dissolution and subsequently driven microbialite accretion and lithification (Allen et al., 2009; Goh et al., 2009). Both "*Gakhumella*" columns and various spheroids therefore may have strongly involved the accretion processes of the Xiajiacao stromatolites and thrombolites.

5.3. Growth and demise of the Xiajiacao microbialite

After the end-Permian regional regression bracketed the irregular contact above Bed 1, a low-relief stromatolite layer grew during the initial stage of a new transgression (Fig. 2). The "cabbage-like" and columnar morphology as well as fragmented columnar sediments within stromatolite may indicate a relatively shallow, high-energy environment, i.e., upper subtidal zone (Fig. 2). Regionally, this layered stromatolite and its equivalents are absent in most PTBM sections, South China (Kershaw et al., 2012), and occur in only a few sites, such as the Yudongzi section of Jiangyou, Sichuan Province (Tang et al., 2017), the Chongyang section, Hubei Province (Yang et al., 2011; Adachi et al., 2017), and the Zuodeng section of Guangxi Province (Fang et al., 2017a). Thus, we suggest that stromatolite grew first in most

areas in South China, but later were eroded during the initial transgression (Fang et al., 2017a). The overlying dolomitic limestone contains extensive fine-grained sediment (Fig. 4B), and thus may represent a slightly lower energy, but deeper habitat in comparison with the stromatolite layer (Fig. 2).

In comparison, the lack of hydrodynamic structures, massive character, thick bedding, and mud-rich texture in thrombolite perhaps indicate a relatively lower energy lower subtidal zone (Fig. 2). It should be noted that thrombolite in Bed 5 yields a much more abundant and diverse metazoan shell beds than Bed 4 and Bed 6, pointing to a slightly shallower habitat, but still within lower subtidal zone (Fig. 2).

The termination of the post-extinction thrombolites is interpreted to have occurred by continued transgression. The capping wackestone and mudstone with horizontal laminae indicates a lower-energy habitat. However, the presence of pelagic conodonts indicates a rise in sea-level above the microbialites and, instead, suggests a deeper setting. The likelihood of a regional sea-level rise is also indicated by both sedimentary and paleoecologic evidence from the conodonts *I. staeschei* Zone to *I. isarcica* Zone in the Meishan section, South China (Wignall and Hallam, 1993; Chen et al., 2002, 2015; Tian et al., 2014). If so, the succession from microbialite to capping wackestone and mudstone reflects a transgressive process, and the Xiajiacao microbialite ceased its growth due to a continuous rise in sea-level.

In addition, the capping wackestone and mudstone above the microbialite may also indicate an increase in terrestrial sediment supplies. Similarly, conodont rare earth elements of conodont bioapatite indicate that terrestrial chemical weathering increased significantly in coincidence with the *I. staeschei* Zone (Zhao et al., 2013). Thus, the elevated chemical weathering on land caused the increased supplies of terrestrial sediments. The injection of terrestrial sediments (i.e., muddy sediments)

may have inhibited the growth of microbialite. Accordingly, the demise of the Xiajiacao microbialite likely resulted from both the increased supplies of terrestrial sediments and sea-level rise (Fig. 2).

5.4. Felsic volcanisms

The P–Tr boundary volcanic ash beds and tuffs are widely distributed in South China. The typical volcanic ash-sourcing quartz crystals are usually bipyramidal-shaped β-quartz (Yang et al., 1991; Yin et al., 1992; Zhang et al., 2006), which, when preserved in association with microspheroids, shows sharp edges (Smyth et al., 2008). The Xiajiacao micro-quartz grains not only exhibit crystal forms similar to β-quartz, but also show sharp edges, characteristic of volcanically derived micro-quartz particles (Fig. 10E–H, L). Rounded quartz grains containing extremely high SiO_2 content (Fig. 10I, M) are also of volcanic origin (Zhang et al., 2014). Their surfaces are also affected by erosion, or possible melting representing a relatively high temperature condition (Fig. 10G).

Volcanic quartz grain abundance shows a pronounced peak in the uppermost skeletal packstone unit, ~20 centimeters below the mass extinction horizon, then abruptly drops near the extinction horizon (Fig. 2). This means that felsic volcanic eruption peak predated biotic mass extinction, unlike volcanic ashes recorded in the Meishan GSSP where the volcanic ash bed (Bed 25)is associated with biotic extinction (Jin et al., 2000). In Xiajiacao, the relatively low contents of volcanic quartz grains occur in the strata of top 20 centimeters in skeletal packstone. This is probably because the topmost skeletal packstone represents a shallow, high-energy, agitated habitat due to the regional regression in that time (Fig. 2), and volcanic ashes

and grains could not be deposited in such an agitated environment. Alternatively, quartz grains may have deposited earlier, but were later eroded due to the regional regression corresponding to the irregular contact between Permian skeletal packstone and overlying microbialite (Yin et al., 2014; Fang et al., 2017a; this study).

As analyzed above, most parts of the Xiajiacao microbialite were deposited in relatively low-energy condition, which is a suitable depositional environment for quartz grains to deposit. The low contents of volcanic quartz grains throughout the microbialite and overlying wackestone and mudstone indicate that volcanic eruption was not active in that time because these sediments mostly represent the relatively low-energy environment. The new finding therefore does not support the idea that volcanic eruption facilitated microbial bloom in the earliest Triassic (Xie et al., 2010), at least in this area, probably because felsic volcanic eruptions may have not stimulated microbial proliferation immediately. Instead, microbes bloomed ~30 kyr after the intensive volcanic eruption following the duration estimate of Beds 25–27 in the Meishan GSSP (Burgess et al., 2014; Chen et al., 2015).

5.5. Redox conditions of microbialites

Modern Black Sea oceanography shows that there is potential for microbe-rich water to move vertically from the lower to upper ocean (Kershaw, 2015), strengthening the earlier idea that the PTBM was driven by upwelling of oxygen-poor carbonate-saturated deep-ocean waters. However, the limited occurrence of precipitated carbonate fans, together with recent evidence that the oceans may have been stratified, cause problems for this model (Kershaw et al., 2012).

Within the Xiajiacao microbialite succession, framboids from most horizons

show mean diameters of 8–12 μm except for Bed 3 having framboids with a mean diameter of 6 μm, which points to an anoxic to lower dyoxic condition. The mean diameter of all microbialite framboids is 9.43 μm (Figs. 2, 10A–D), and the crossplot suggests a dysoxic condition for all horizons (Fig. 11). Both framboid sizes and morphology, overall, show that most microbialite horizons may represent a lower to upper dysoxic condition.

Pyrite framboids from the basal microbialite unit (Beds 2-4) generally show relatively lower values in diameter, indicating a possible lower dysoxic condition. Bed 5 may represent an upper dysoxic condition due to elevated framboid sizes and a diverse metazoan assemblage of ostracods, brachiopods, gastropods, and microconchids (Fig. 5D–F). Interestingly, most spheroids are also associated with relatively large framboids in the examined strata. Framboids from the upper part of Bed 6 show decreasing sizes again, and those from the capping wackestone and mudstone point to an anoxic to lower dysoxic condition (Fig. 2) probably due to the rapid rise in sea-level.

Overall, the Xiajiacao stromatolite and thrombolite, may have been deposited in a lower to upper dysoxic condition, which is in line with the sedimentary environment of the *H. parvus* conodont Zone (Bed 27c) in the Meishan GSSP (Chen et al., 2015; Huang et al., 2017), noting of course that the sediments of the Meishan GSSP were deposited in deeper waters, and also lack any microbialites.

Despite the indications of lowered oxygenation of the water in which the microbialite grew, there are at least two other possible explanations of framboids in the microbialite: 1) pulses of upwelling of large masses of anoxic water from the deeper ocean below the redox boundary onto the shelf. The potential exists for framboids to be swept up with upwelled water and deposited amongst microbialites

and shelly faunas. Thus if microbialites and shelly faunas that grew in oxygenated water were inundated by anoxic waters carrying framboids, then the potential for mixing of anoxic water with oxygen-requiring organisms. 2) the framboids formed diagenetically in the sediment below the redox boundary, where the water above was oxygenated, followed by storm action to mix and rapidly deposit framboids along with microbialite and shells, mixing anoxic and oxic components. Rapid burial would have been necessary to avoid oxidation of the framboids.

It should also be noted that, so far, no framboids were derived from fossil shell concentrations within the microbialite. Even so, most shells are unevenly preserved and moderately fragmented. They therefore could have lived in dysoxic to oxic habitats, but later were slightly transported and re-deposited mixed with framboids.

With respect to the redox conditions of other PTBMs in South China, they are very different from place to place based on either ostracod paleoecology, pyrite framboid size and morphology or cerium anomaly. The ostracod assemblage indicates that microbialites from the Chongyang locality of Hubei Province and some isolated platforms within the Nanpanjiang Basin, Guizhou Province formed in a well-oxygenated habitat (Liu et al., 2010; Forel et al., 2009), but limited samples from the Laolongdong locality of Sichuan Province suggest that those grew in an anoxic to dysoxic condition (Crasquin-Soleau and Kershaw, 2005). Alternatively, abundant tiny pyrite framboids (<5 μm in diameter) have been detected in the Chongyang, Cili (Wang et al., 2016), Laolongdong (Liao et al., 2010), and Ziyun (Wu et al., 2007) localities, and in Nanpanjiang Basin microbialites (Ezaki et al., 2008; Yang et al., 2011). Such small-sized pyrite framboids grew in an anoxic location (Bond and Wignall, 2010; Kershaw, 2015; Huang et al., 2017), although they could be transported to an oxygenated habitat (Kershaw, 2015) if the transport and burial were

sufficiently rapid to prevent framboid oxidation. Loope et al. (2013) argued that the Cili microbialite was deposited in an oxic environment based on Cerium anomaly in rare earth element.

To sum, if considering various redox conditions revealed by different proxies for the PTBMs in South China, there is currently insufficient information available to determine whether the PTBMs grew in fully oxygenated or lowered oxygen conditions. However, results from paleoecologic, pyrite framboid, and geochemical analyses suggest that oxygen levels may have been less important to the growth of PTBMs than has been considered by current published work (Wu et al., 2017). Further work for additional PTBMs are necessary to investigate these ideas further.

6. Conclusions

An integration of detailed petrologic study, microanalysis, and pyrite framboid analysis on the newly found the P–Tr boundary microbialite in western Hubei Province, South China achieves the following new observations:

(1) "*Gakhumella*", coccoid-like spheroids, bacterial clump-like spheroids, and hollow spheroids are abundant in the stromatolite and thrombolite, and probably have played an important role in accretion of the microbialites in this site;

(2) It has not been possible to determine whether the pronounced irregular contact beneath the microbialites was caused by submarine solution in the wake of ocean acidification or subaerial exposure due to regional regression.

(3) Pyrite framboid size and morphology show that the microbialite may have been deposited in lower to upper dysoxic conditions. However, framboids are not fully confirmed to indicate redox condition of microbialite due to multiple

possibilities for interpreting the occurrence of framboids in microbialite.

(4) Stratigraphic abundance of β-quartz and glassy grains shows that either intensive volcanic eruption only occurred just prior to biotic extinction or volcanism was intensive during biotic extinction, but volcanic grains were not deposited due to the shallow, agitated environment caused by the regional regression. Microbial bloom, indicated by the widespread PTBMs seems not to be linked with the contemporaneous volcanism.

Acknowledgements

We thank both anonymous reviewers and editor Thomas Algeo for critical comments and constructive suggestions, which have greatly improved the quality of the paper. This study is partly supported by the 111 Program of China (B08030), two NSFC grants (41572091, 41402089), and one research grant from the State Key Laboratory of Biogeology and Environmental Geology (BGEG), China University of Geosciences (GBL11206). It is a contribution to the IGCP 630 "Permian–Triassic climatic and environmental extremes and biotic response".

References

Adachi, N., Asada, Y., Ezaki, Y., Liu, J.B., 2017. Stromatolites near the Permian–Triassic boundary in Chongyang, Hubei province, South China: A geobiological window into palaeo-oceanic fluctuations following the end-Permian extinction. Palaeogeogr. Palaeoclimatol. Palaeoecol. 475, 55–69.

Adachi, N., Ezaki, Y., Liu, J.B., 2004. The fabrics and origins of peloids immediately after the end-Permian extinction, Guizhou Province, South China. Sediment. Geol. 164, 161–178.

Allen, M.A., Goh, F., Burns, B.P., Neilan, B.A., 2009. Bacterial, archaeal and eukaryotic diversity of smooth and pustular microbial mat communities in the hypersaline lagoon of Shark Bay. Geobiology 7, 82–96.

Bond, D.P.G., Wignall, P.B., 2010. Pyrite framboid study of marine Permian–Triassic boundary sections: A complex anoxic event and its relationship to contemporaneous mass extinction. Geol. Soc. Am. Bull. 122, 1265–1279.

Bosak, T., Souza-Egipsy, V., Newman, K., 2004. A laboratory model of abiotic peloids formation. Geobiology 2, 189–198.

Bottjer, D.J., Clapham, M.E., Fraiser, M.L., Powers, C.M., 2008. Understanding mechanisms for the end-Permian mass extinction and the protracted Early Triassic aftermath and recovery. GSA Today 18, 4–10.

Burgess, S.D., Bowring, S., Shen, S.Z., 2014. High-precision timeline for Earth's most severe extinction. Proc. Nat. Acad. Sci. U.S.A. 111, 3316–3321.

Chafetz, H.S., 1986. Marine peloids: a product of bacterially induced precipitation of calcite. J. Sediment. Petrol. 56, 812–817.

Chafetz, H.S., Folk, R.L., 1984. Travertines: depositional morphology and the

bacterially constructed constituents. J. Sediment. Petrol. 54, 289–316.

Chen, L., Wang, Y.B., Xie, S.C., Kershaw, S., Dong, M., Yang, H., Liu, H., Algeo, T.J., 2011. Molecular records of microbialites following the end-Permian mass extinction in Chongyang, Hubei Province, South China. Palaeogeogr. Palaeoclimatol. Palaeoecol. 308, 151–159.

Chen, Z.Q., Benton, M.J., 2012. The timing and pattern of biotic recovery following the end-Permian mass extinction. Nat. Geosci. 5, 375–383.

Chen, Z.Q., Shi, G.R., Kaiho, K., 2002. A new genus of rhynchonellid brachiopod from the Lower Triassic of South China and implications for timing the recovery of Brachiopoda after the end-Permian mass extinction. Palaeontology 45, 149–164.

Chen, Z.Q., Wang, Y.B., Kershaw, S., Luo, M., Yang, H., Zhao, L.S., Fang, Y.H., Chen, J.B., Yang, L., Zhang, L., 2014. Early Triassic stromatolites in a siliciclastic nearshore setting in northern Perth Basin, Western Australia: geobiologic features and implications for post-extinction microbial proliferation. Glob. Planet. Chang. 121, 89–100.

Chen, Z.Q., Yang, H., Luo, M., Benton, M.J., Kaiho, K., Zhao, L.S., Huang, Y.G., Zhang, K.X., Fang, Y.H., Jiang, H.S., Qiu, H., Li, Y., Tu, C.Y., Shi, L., Zhang, L., Feng, X.Q., Chen, L., 2015. Complete biotic and sedimentary records of the Permian–Triassic transition from Meishan section, South China: Ecologically assessing mass extinction and its aftermath. Earth-Sci. Rev. 149, 67–107.

Clarkson, M.O., Kasemann, S.A., Wood, R.A., Lenton, T.M., Daines, S.J., Richoz, S., Ohnemueller, F., Meixner, A., Poulton, S.W., Tipper, E.T., 2015. Ocean acidification and the Permo–Triassic mass extinction. Science 348, 229–232.

Collin, P.Y., Kershaw, S., Soleau, S.C., Feng, Q., 2009. Facies changes and diagenetic

processes across the Permian–Triassic boundary event horizon, Great Bank of Guizhou, South China: A controversy of erosion and dissolution. Sedimentology 56, 677–693.

Crasquin–Soleau, S., Kershaw, S., 2005. Ostracod fauna from the Permian–Triassic boundary interval of South China (Huaying Mountains, eastern Sichuan Province): palaeoenvironmental significance. Palaeogeogr. Palaeoclimatol. Palaeoecol. 217, 131–141.

Cui, Y., Kump, L.R., Ridgewell, A., 2013. Initial assessment of the carbon emission rate and climatic consequences during the end-Permian mass extinction. Palaeogeogr. Palaeoclimatol. Palaeoecol. 389, 128–136.

De Castro, P., 1969. Su alone tallofite del Mesozoico in Campania. Strtigrafia e Paleontologia, Bollettino della Società dei naturalisti in Napoli 78, 87–167.

Dupraz, C., Pamela, R.R., Braissant, O., Decho, A.W, Norman, R.S., Visscher, P.T., 2009. Processes of carbonate precipitation in modern microbial mats. Earth-Sci. Rev. 96, 141–162.

Erwin, D.H., 2006. Extinction: How life on Earth nearly ended 250 million years ago. Princeton University Press, Princeton, pp. 1–296.

Ezaki, Y., Liu, J., Adachi, N., 2003. Earliest Triassic microbialite micro to megastructures in the Huaying area of Sichuan Province, South China: implications for the nature of oceanic conditions after the end-Permian extinction. PALAIOS 18, 388–402.

Ezaki, Y., Liu, J., Nagano, T., Adachi, N., 2008. Geobiological aspects of the earliest Triassic microbialites along the southern periphery of the tropical Yangtze Platform: Initiation and cessation of a microbial regime. Palaeogeogr. Palaeoclimatol. Palaeoecol. 23, 356–369.

Ezaki, Y., Liu, J.B., Adachi, N., 2012. Lower Triassic stromatolites in Luodian County, Guizhou Province, South China: Evidence for the protracted devastation of the marine environments. Geobiology 10, 48–59.

Fang, Y.H., Chen, Z.Q, Kershaw, S., Y, H., Luo, M., 2017a. Permian–Triassic boundary microbialites at Zuodeng Section, Guangxi Province, South China: Geobiology and palaeoceanographic implications. Glob. Planet. Chang. 152, 115–128.

Fang, Q., Hong, H.L., Chen, Z.Q, Yu, J.X., Wang, C.W., Yin, K., Zhao, L.L., Liu, Z., Cheng, F., Gong, N.N, Furnes, H., 2017b. Microbial proliferation coinciding with volcanism during the Permian–Triassic transition: New, direct evidence from volcanic ashes, South China. Palaeogeogr. Palaeoclimatol. Palaeoecol. (in press).

Feng, Z., Yang, Y., Jin, Z., 1997. Lithofacies Paleogeoraphy of Permian of South China. China University of Petroleum Press, Beijing (82 pp) (in Chinese).

Folk, R.L., Chafetz, H.S., 2000. Bacterially induced microscale and nanoscale carbonate precipitates. In: Microbial sediments. Springer, Berlin, pp. 40–49.

Forel, M.B., 2013. The Permian–Triassic mass extinction: Ostracods (Crustacea) and microbialites. C.R.Geosci.345, 203–211.

Forel, M.B., Crasquin, S., Kershaw, S., Feng, Q.L., Collin, P.Y., 2009. Ostracods (Crustacea) and water oxygenation in the earliest Triassic of South China: implications foroceanic events at the end–Permian mass extinction. Aust. J. Earth Sci. 56, 815–823.

Forel, M.B., Crasquin, S., Kershaw, S., Collin, P.Y., 2012. In the aftermath of the end-Permian extinction: The microbialite refuge? Terra Nova 25, 137–143.

Gao, Q.L., Chen, Z.Q., Zhang, N., Griffin, W.L., Xia, W.C., Wang, G.Q., Jiang, T.F.,

Xia, X.F., O'Reilly, S.Y., 2015.Ages, trace elements and Hf-isotopic compositions of zircons from claystones around the Permian–Triassic boundary in the Zunyi section, South China: Implications for nature and tectonic setting of the volcanism. J. Earth Sci. 26, 872–882.

Gao, Q.L., Zhang, N., Xia, W.C., Feng, Q.L., Chen, Z.Q., Zheng, J.P., Griffin, W.L., O'Reilly, S.Y., Pearson, N.J., Wang, G.Q., Wu, S., Zhong, W.L., Sun, X.F., 2013. Origin of volcanic ash beds across the Permian–Triassic boundary, Daxiakou, South China: Petrology and U–Pb age, trace elements and Hf-isotope composition of zircon. Chem. Geol. 360, 41–53.

Goh, F., Allen, M.A., Leuko, S., Kawaguchi, T., Decho, A.W., Burns, B.P., Neilan, B.A., 2009. Determining the specific microbial populations and their spatial distribution within the stromatolite ecosystem of Shark Bay. ISME Journal 3, 383–396.

Hethke, M., Fürsich, F.T., Jiang, B., Klaus, R., 2013. Oxygen deficiency in Lake Sihetun Formation of the Lower Cretaceous Liaoning Fossil lagerstätte (China). J. Geol. Soc. 170, 817–831.

Hinojosa, J.L., Brown, S.T., Chen, J., DePaolo, D.J., Paytan, A., Shen, S.Z., Payne, J.L., 2010. Evidence for end-Permian ocean acidification from calcium isotopes in biogenic apatite. Geology 40, 743–746.

Huang, Y.G., Chen, Z.Q., Wignall, P.B., Zhao, L.S., 2017. Latest Permian to Middle Triassic redox condition variations in ramp settings, South China: Pyrite framboid evidence. Geol. Soc. Am. Bull. 129, 229–243.

Hughes, G.W., 2010. Calcimicrobe tubules in uppermost Jurassic Arab—A carbonates of Saudi Arabia. GeoArabia 15, 17–26.

Hughes, G.W., 2013. Late Permian to Late Jurassic "microproblematica" of Saudi

Arabia: Possible palaeobiological assignments and roles in the palaeoenvironmental reconstructions. GeoArabia 18, 57–92.

Jiang, H.S., Lai, X.L., Sun, Y.D., Wignall, P.B., Liu, J., Yan, C., 2014. Permian–Triassic conodonts from Dajiang (Guizhou, South China) and their implication for the age of microbialite deposition in the aftermath of the end-Permian mass extinction. J. Asian Earth Sci. 25, 413–430.

Jin, Y.G., Wang, Y., Wang, W., Shang, Q.H., Cao, C.Q., Erwin, D.H., 2000. Pattern of marine mass extinction near the Permian–Triassic boundary in South China. Science 289, 432–436.

Kazmierczak, J., Coleman, M.L, Gruszczynski, M., Kempe, S., 1996. Cyanobacterial key to the genesis of micritic and peloidal limestones in ancient seas. Acta Palaeontologica Polonica 41, 319–338.

Kershaw, S., 2015. Modern Black Sea oceanography applied to the end-Permian extinction event. J. Paleogeogr. 4, 52–62.

Kershaw, S., Zhang, T., Lan, G., 1999. A ?microbialite crust at the Permian–Triassic boundary in South China, and its palaeoenvironmental significance. Palaeogeogr. Palaeoclimatol. Palaeoecol. 146, 1–18.

Kershaw, S., Guo, L., Swift, A., Fan, J., 2002. ?Microbialites in the Permian–Triassic boundary interval in central China: Structure, age and distribution. Facies 47, 83–90.

Kershaw, S., Li, Y., Crasquin, S., Feng, Q., Mu, X., Collin, P.Y, Reynolds, A., Guo, L., 2007. Earliest Triassic microbialites in the South China block and other areas: Controls on their growth and distribution. Facies 53, 409–425.

Kershaw, S., Crasquin, S., Li, Y., Collin, P.Y., Forel, M.B., Mu, X., Baud, A., Wang, Y., Xie, S., Maurer, F., Guo, L., 2012. Microbialites and global environmental

change across the Permian–Triassic boundary: A synthesis. Geobiology 10, 25–47.

Kershaw, S., Collin, P.Y., Crasquin, S., 2016. Comment to Lehrmann et al. New sections and observations from the Nanpanjiang Basin, South China. PALAIOS 31, 111–117.

Krull, E.S., Lehrmann, D.J., Druke, D., Kessel, B., Yu, Y.Y., Li, R.X., 2004. Stable carbon isotope stratigraphy across the Permian–Triassic boundary in shallow marine carbonate platforms, Nanpanjiang Basin, South China. Palaeogeogr. Palaeoclimatol. Palaeoecol. 204, 297–315.

Lehrmann, D.J., 1999. Early Triassic calcimicrobial mounds and biostromes of the Nanpanjiang Basin, South China. Geology 27, 359–362.

Lehrmann, D.J., Bentz, J. M., Wood, T., Goers, A., Dhillon, R., Akin, S., Li, X.W., Payne, J.L., Kelley, B.M., Meyer, K.M., Schaal, E.K., Suarez, M.B., Yu, M.Y., Qin, Y.J., Li, R.X., Minzoni, M., Henderson, C.M., 2015. Environmental controls on the genesis of marine microbialites and dissolution surface associated with the end-Permian mass extinction: New sections and observations from the Nanpanjiang Basin, South China. PALAIOS 30, 529–552.

Liao, W., Wang, Y.B., Kershaw, S., Weng, Z.T., Yang, H., 2010. Shallow-marine dysoxia across the Permian–Triassic boundary: Evidence from pyrite framboids in the microbialite in South China. Sediment. Geol. 232, 77–83.

Liu, H., Wang, Y.B., Yuan, A.H., Yang, H., Song, H.J., Zhang, S.X., 2010. Ostracod fauna near the Permian–Triassic boundary in Chongyang, Hubei Province, and its response to the mass extinction. Sci. Chin. Ser. D: Earth Sci. 53, 810–817.

Liu, J.B., Ezaki, Y., Yang, S.R., Wang, H.F., Adachi, N., 2007. Age and sedimentology of microbialites after the end-Permian mass extinction in Luodian, Guizhou

Province. J. Palaeogeogr. 9, 473–486 (in Chinese).

Liu, L.J., Jiang, H.X., Wu, Y.S., Cai, C.F., 2014. Community replacement sequences and paleoenvironmental changes in reef areas of South China from Late Permian to Early Triassic exemplified by Panlongdong section in northeastern Sichuan Basin. Sci. China Ser. D Earth Sci. 57, 1093 – 1108.

Loope, G.R., Kump, L.R., Arthur, M.A., 2013. Shallow water redox conditions from the Permian–Triassic boundary microbialite: The rare earth element and iodine geochemistry of carbonates from Turkey and South China. Chem. Geol. 351, 195–208.

Luo, M., Chen, Z.Q., Zhao, L.S., Kershaw, S., Huang, J.Y., Wu, L.L., Yang, H., Fang, Y.H., Huang, Y.G., Zhang, Q.Y., Hu, S.X., Zhou, C.Y., Wen, W., Jia, Z.H., 2014. Early Middle Triassic stromatolites from the Luoping area, Yunnan Province, Southwest China: Geologic features and environmental implications. Palaeogeogr. Palaeoclimatol. Palaeoecol. 412, 124–140.

Luo, M., Chen, Z.Q., Shi, G.R., Fang, Y.H., Song, H. J., Jia, Z.H., Huang, Y.G., Yang, H., 2016. Late Early Triassic stromatolite from Anhui, South China: Geobiologic features and palaeoenvironmental implication. Palaeogeogr. Palaeoclimatol. Palaeoecol. 452, 40–54.

Mastandrea, A., Perri, E., Russo, F., Spadafora, A., Tucker, M., 2006. Microbial primary dolomite from a Norian carbonate platform: Northern Calabria, southern Italy. Sedimentology 53, 465–480.

Mu, X.N., Kershaw, S., Li, Y., Guo, L., Qi, Y.P., Reynolds, A., 2009. High-resolution carbon isotope changes in the Permian–Triassic boundary interval, Chongqing, South China; implications for control and growth of earliest Triassic microbialites. J. Asian Earth Sci. 36, 434–441.

Payne, J.L., Lehrmann, D.J., Follett, D., Seibel, M., Kump, L.R., Riccardi, A., Altiner, D., Sano, H., Wei, J., 2007. Erosional truncation of uppermost Permian shallow-marine carbonates and implications for Permian–Triassic boundary events. Geol. Soc. Am. Bull. 119, 771–784.

Payne, J.L., Lehrmann, D.J., Follett, D., Seibel, M., Kump, L.R., Riccardi, A., Altiner, D., Sano, H., Wei, J., 2009. Erosional truncation of uppermost Permian shallow-marine carbonates and implications for Permian–Triassic boundary events: Reply. Geol. Soc. Am. Bull. 121, 957–959.

Payne, J.L., Turchyn, A.V., Payton, A., DePaolo, D.J., Lehrmann, D.J., Yu, M.Y., Wei, J., 2010. Calcium isotope constraints on the end-Permian mass extinction. Proc. Nat. Acad. Sci. U.S.A. 19, 8543–8548.

Perri, E., Tucker, M., 2007. Bacterial fossils and microbial dolomite in Triassic stromatolites. Geology 35, 207–210.

Reitner, J., 1993. Modern cryptic microbialite/metazoan facies from Lizard Island (Great Barrier Reef, Australia)—formation and concepts. Facies, 29, 3–40.

Reitner, J., Neuweiler, F., 1995. Mud mounds: A polygenetic spectrum of fine-grained carbonate buildups. Facies 32, 1–70.

Smyth, H.R., Hall, R., Nichols, G.J., 2008. Significant volcanic contribution to some quartz-rich sandstones, east Java, Indonesia. J. Sediment. Res. 78, 335–356.

Song, H.J, Tong, J.N, Chen, Z.Q., Yang, H., Wang, Y.B., 2009. End-permian mass extinction of foraminifers in the Nanpanjiang Basin, South China. Journal of Paleontology 83, 718–738.

Tang, H., Kershaw, S., Liu, H., Tan, X.C., Li, F., Hu, G., Huang, C., Wang, L.C., Lian, C.B., Li, L., Yang, X.F., 2017. Permian–Triassic boundary microbialites (PTBMs) in southwest China: implications for paleoenvironment reconstruction.

Facies 63, 2.

Tian, S.F., Chen, Z.Q., Huang, C.J., 2014. Orbital forcing and sea-level changes in the earliest Triassic of the Meishan section, South China. J. Earth Sci. 25, 64–73.

Tribovillard, N.P., 1998. Cyanobacterially generated peloids in laminated, organic-matter rich, limestones: an unobtrusive presence. Terra Nova 10, 126–130.

Wang, Y.B., Tong, J., Wang, J.S., Zhou, X.G., 2005. Calcimicrobialite after end-Permian mass extinction in South China and its palaeoenvironmental significance. Chin. Sci. Bull. 50, 665–671.

Wang, L.N., Wignall, P.B., Wang, Y.B., Jiang, H.S., Sun, Y.D., Li, G.S., Yuan, J.L., Lai, X.L., 2016. Depositional conditions and revised age of the Permo–Triassic microbialites at Gaohua section, Cili Country (Hunan Province, South China). Palaeogeogr. Palaeoclimatol. Palaeoecol. 443, 156–166.

Wignall, P.B., Hallam, A.J., 1993. Griesbachian (earliest Triassic) palaeoenvironmental changes in the Salt Range, Pakistan and southeast China and their bearing on the Permo–Triassic mass extinction. Palaeogeogr. Palaeoclimatol. Palaeoecol. 102, 215–237.

Wignall, P.B., Kershaw, S., Collin, P.Y., Crasquin-Soleau, S., 2009. Comment: erosional truncation of uppermost Permian shallow-marine carbonates and implications for Permian–Triassic boundary events. Geol. Soc. Am. Bull. 121, 954–956.

Wilkin, R.T., Barnes, H.L., Brantley, S.L., 1996. The size distribution of framboidal pyrite in modern sediments: An indicator of redox conditions. Geochim. Cosmochim. Ac. 60, 3897–3912.

Wu, S.Q., Chen, Z.Q, Fang, Y.H., Pei, Y., Yang, H., 2017. A Permian–Triassic boundary microbialite deposit from the eastern Yangtze Platform (Jiangxi

Province, South China): Geobiologic features, ecosystem composition, and redox conditions. Palaeogeogr. Palaeoclimatol. Palaeoecol.(in press).

Wu, Y.S., Jiang, H.X., Yang, W., Fan, J.S., 2007. Microbialite of anoxic condition from Permian–Triassic transition in Guizhou, China. Sci. Chin. D: Earth Sci. 50, 1040–1051.

Wu, Y.S., Yu, G.L., Li, R.H., Song, L.R., Jiang, H.X., Riding, R., Liu, L.J., Liu, D.Y., Zhao, R., 2014. Cyanobacterial fossils from 252 Ma old microbialites and their environmental significance. Sci. Rep. 4, 3820–3824.

Xie, S.C., Pancost, R.D., Wang, Y.B., Yang, H., Wignall, P. B., Luo, G.M., Jia, C.L., Chen.L., 2010. Cyanobacterial blooms tied to volcanism during the 5 m.y. Permo-Triassic biotic crisis. Geology 38, 447–450.

Yang, H., Wang, Y.B., Chen, L., 2008. Occurrence of organic matter in calcimicrobialites across Permian–Triassic boundary in Huayingshan region, Sichuan, South China. Journal of China University of Geosciences 19, 518–525.

Yang, H., Chen, Z.Q., Wang, Y.B., Tong, J.N., Song, H.J., Chen, J., 2011. Composition and structure of microbialite ecosystems following the end-Permian mass extinction in South China. Palaeogeogr. Palaeoclimatol. Palaeoecol. 308, 111–128.

Yang, H., Chen, Z.Q., Ou, W.Q., 2015a. Microconchids from microbialites near the Permian–Triassic boundary in the Zuodeng section, Baise area, Guangxi Province, South China and their palaeoenvironmental implications. J. Earth Sci. 26, 157–1965.

Yang. H., Chen, Z.Q., Wang, Y.B., Ou, W.Q., Liao, W., Mei, X., 2015b. Palaeoecology of microconchids from microbialites near the Permian–Triassic boundary in South China. Lethaia 48, 497–508.

Yang, Z.Y., Wu, S.B., Yin, H.F., Xu, G.R., Zhang, K.X., 1991. Geological events during Permian and Triassic transition in South China. Geological publishing house, Beijing, pp. 35–63 (in Chinese).

Yin, H.F., Huang, S.J., Zhang, K.X., 1992. The effects of volcanism on the Permo–Triassic mass extinction in South China. In: Sweet, W.C., Yang, Z.Y., Dickins, J.M., Yin, H.F. (Eds), Permo–Triassic Events in the Eastern Tethys. Cambridge University Press, London, pp.146–157.

Yin, H.F., Jiang, H.S., Xia, W.C., Feng, Q.L., Zhang, N., Shen, J., 2014. The end-Permian regression in South China and its implication on mass extinction. Earth Sci. Rev. 137, 19–33.

Yu, C., 2015. Study on the sedimentary facies of Permian–Triassic boundary section in Lichuan, Western Hubei. Master Degree Dissertation (in Chinese).

Yu, C., Yao, H.Z., Zhao, X.M., Yang, Z.Q., 2015. Carbonate microfacies in strata near the Permian–Triassic boundary and the volcanic activity evidence in the early Triassic in Lichuan area, Western Hubei Province. Geology and Mineral Resources of South China 31(2), 115–124 (in Chinese).

Zaninetti, L., 1978. Un organisme incertae sedis nouveau dans le Permien supérieur du Sud-Zagros, Iran. Note du Laboratoire de Paléontologie de l‟Université de Genève 3, 17–19.

Zhang, H., Shen, S.Z., Cao, C.Q., Zheng, Q.F., 2014. Origins of microspherules from the Permian–Triassic boundary event layers in South China. Lithos 204, 246–257.

Zhang, S.X., Peng, Y.Q., Yu, J.X., Lei, X.R., Gao, Y.Q., 2006. Characteristics of claystones across the terrestrial Permian–Triassic boundary: Evidence from the Chahe section, western Guizhou, South China. J. Asian Earth Sci. 27, 358–370.

Zhao, L.S., Chen, Z.Q., Algeo, T.J., Chen, J.B., Chen, Y.L., Tong, J., Gao, S., Zhou, L., Hu, Z.C., 2012. Rare-earth element patterns in conodont albid crowns: Evidence for massive inputs of volcanic ash during the latest Permian biocrisis? Glob. Planet. Chang. 105, 135–151.

Zheng, Q.F., Cao, C.Q., Wang, Y., Zhang, H., Ding, Y., 2016. Microbialite concretions in a dolostone crust at the Permian–Triassic boundary of the Xishan section in Jiangsu Province, South China. Palaeoworld 25, 188–198.

Figure captions:

Fig. 1 A) Geographic map showing the locality of the Xiajiacao section, Lichuan County, western Hubei Province, South China. B) Early Triassic paleogeographical map of South China, with Xiajiacao section situated on the northern margin of the Yangtze Platform (modified from Feng et al., 1997).

Fig. 2 Composite section of the P–Tr succession exposed in the Xiajiacao section showing lithology, C/F (conodont/fusulinid) zonations, number of quartz grains, $\delta^{13}C$ excursion, volcanism intensity, pyrite framboid sizes, occurrence frequency of framboidal pyrite (FFP), frequency of authigenic pyrite (FAP), sea level change. Thrombolite can be divided into three parts based on the relative amount of micritic and sparry calcite. The middle part has relatively lower content of micrite. HT represents high tide. LT represents low tide. FWWB represents fair weather wave base. A represents supratidal zone. B represents intertidal zone. C represents upper subtidal zone. D represents lower subtidal zone. Conodont data and $\delta^{13}C$ excursion are after Yu et al. (2015) and Yu (2015).

Fig. 3 A) The whole view of the microbialite. The hammer is 22cm long. B) Field photo of boxed area in view A, showing the pronounced irregular surface (s) on top of the underlying skeletal packstone. The stromatolite (st) grew immediately on the surface overlain by wedge-shaped finely crystalline dolomitic limestone (fcdl). The coin diameter is 2cm. C–D) Field photo of boxed area in view B, showing the stromatolites on top of latest Permian skeletal packstone. E) Polished slab of thrombolite, showing dark-colored, sparry masses (sp) and light-colored micritic masses (m).

Fig. 4 A) Photomicrograph of the Permian skeletal packstone, with abundant

foraminifers, including *Colaniella* (C), *Ichthyofrondina* (I), *Palaeofusulina* (P). B) Photomicrograph of wedge-shaped finely crystalline dolomitic limestone. C) Photomicrograph of thrombolites, comprising irregular sparitic masses (sp) and micritic clots (m). *Earlandia* (E) is abundant. D–F) Metazoans from micritic calcites (m) of thrombolites, including ostracods, brachiopods, gastropods, and microconchids (mc).

Fig. 5 Photomicrographs showing the details of the pronounced irregular contact surface (s) between latest Permian skeletal packstone and the overlying post-extinction microbialite. A) Photomicrograph showing petrologic features across the irregular contact surface (red triangle indicated). B) Photomicrograph of boxed area in view A, showing skeletal packstone mingling with overlying stromatolite or inter-stromatolite deposits. C–D) Photomicrograph of boxed area in view A, showing the truncated algae or foraminifers in skeletal packstone. E) Photomicrograph of boxed area in view A, showing organisms existed along the contact. F) Photomicrograph of boxed area in view A, showing syntaxial cement (sy) possibly on crinoid fragments in skeletal packstone. G) Photomicrograph of boxed area in view A, showing geopetal sediment (ge) and anisopachous cement (ai) in skeletal packstone. H) Close-up of boxed area in view G showing two generations of cements (c1, c2) as well as anisopachous cement: (1) 10 μm, (2) 40 μm. I) Sketch of view H.

Fig. 6 Photomicrographs of separate and aggregate columnar objects. A–C) straight separate columnar objects. D–E) incurved separate columnar objects, F) columnar objects. G–H) aggregate columnar objects.

Fig. 7 Photomicrographs of spherical objects. A–G) Spherical objects featured of a sparitic calcite nucleus surrounded by micritic sheaths. They can occur

separately or aggregately. H–I) Spherical objects characterized by micritic calcite nuclei coated with sparitic calcite sheaths.

Fig. 8 A–E), G) SEM images of separate columnar objects. Single column has a large, rounded proto-chamber followed by a series of thin segments arching to the same direction. Each individual possesses 10–30 distinct segments with a thin but distinct chamber between two segments. Each chamber is ~2 μm thick, and filled with microsparitic calcite. F) Close-up of boxed area in E, showing separate columnar objects. H) Close-up of boxed area in G, showing separate columnar objects.

Fig. 9 SEM images of three types of spheroids. A) Spherical objects composed of a coarse sparry nucleus coated with radiating rays. B–E) Spherical objects characterized by one rounded nucleus that comprises radiating rays and are surrounded by coarse radial rays. B) The round nucleus is covered by one thin micritic layer, which is pronounced when being well-preserved. C–E) The round nucleus is covered by one thin micritic layer, which disappears when being poorly preserved. F–H) Spherical objectsconsisting of a void nucleus coated with radiating rays.

Fig. 10 A–D) SEM images of pyrite framboids. They may clump together or scatter separately. E–I) SEM images of bipyramid-shaped quartz crystals and glassy balls, ranging from 150 to 250 μm in diameter. G) Close-up of boxed area in F, showing the inflated surfaces that are seriously eroded or melt. J–K) SEM images of phosphates of limes. L) EDS element analysis of bipyramidal-shaped quartz in view E. M) EDS element analysis of rounded quartz in view I. N–O) EDS element analysis of phosphates of limes in view J and K.

Fig. 11 Cross-plot diagram showing mean diameter vs. standard deviation of

framboids. The cross-plot suggests a dysoxic condition.

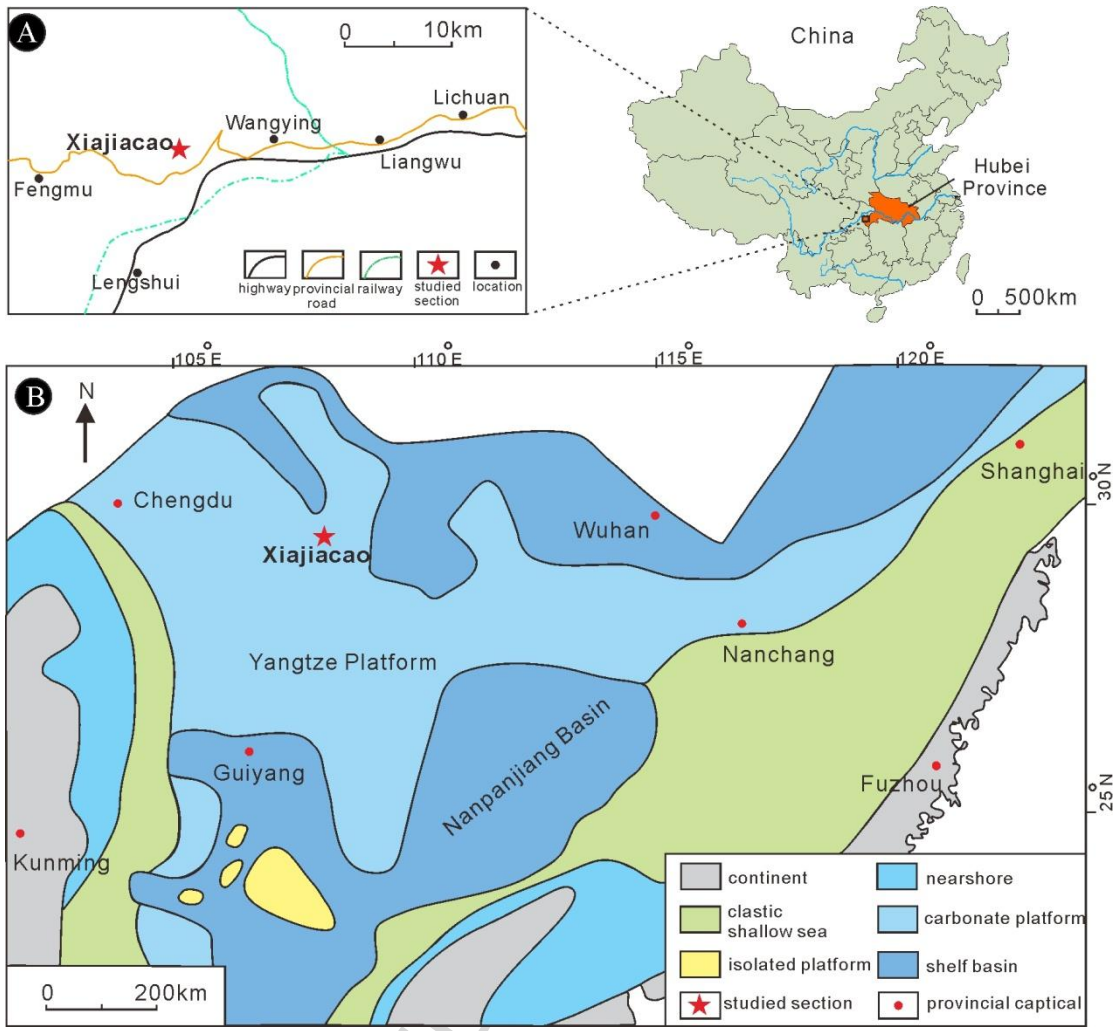

Figure 1

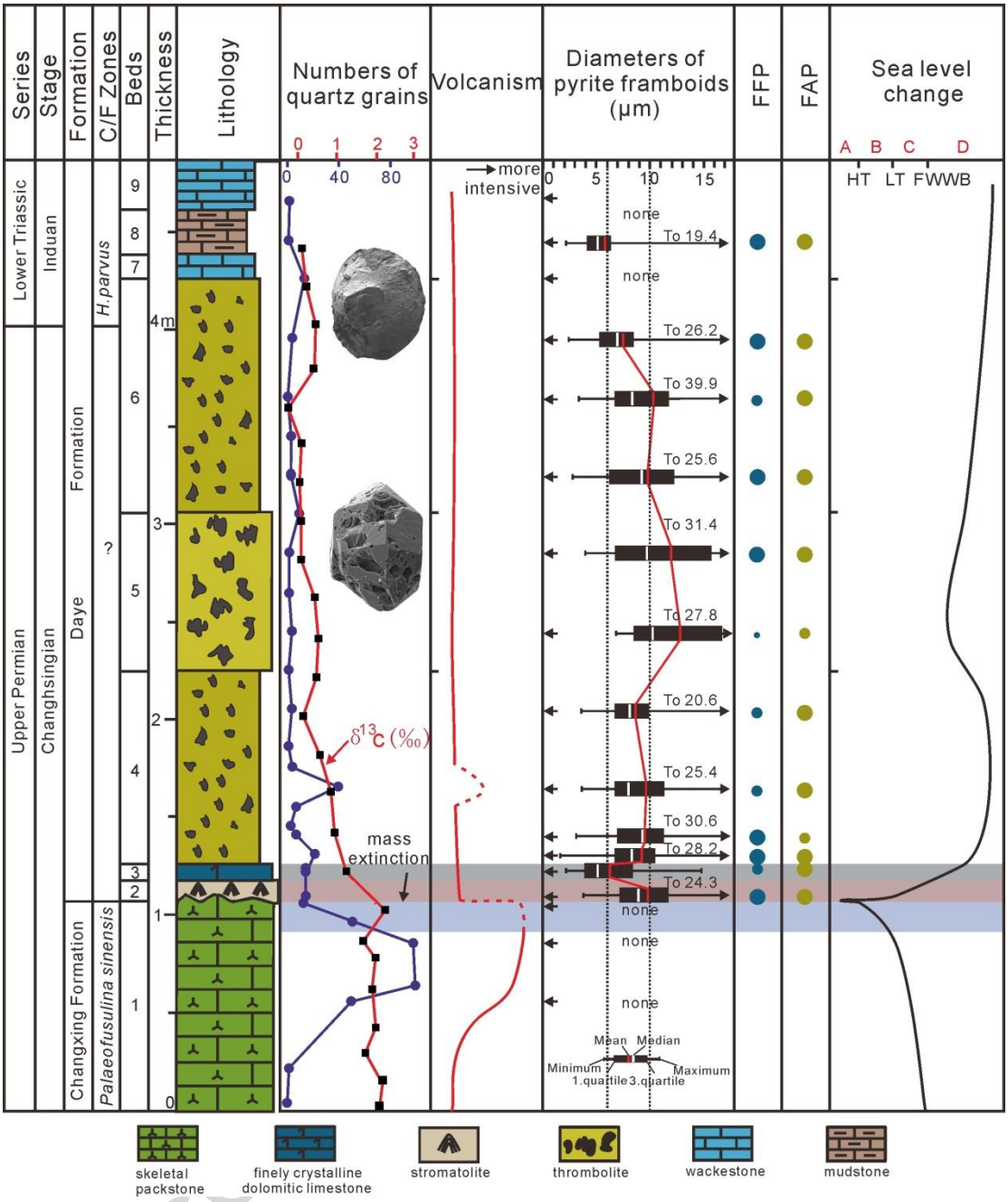

Figure 2

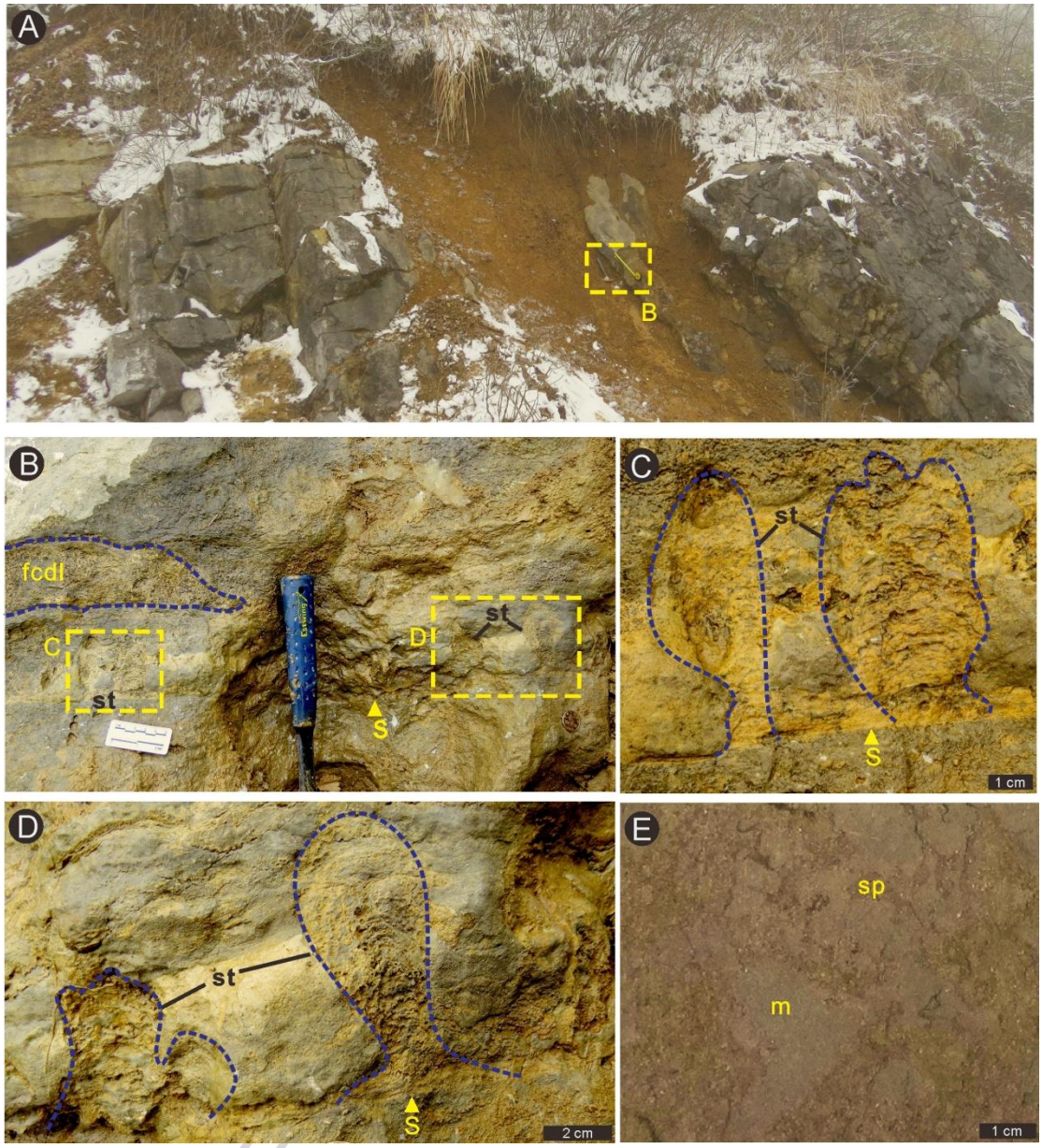

Figure 3

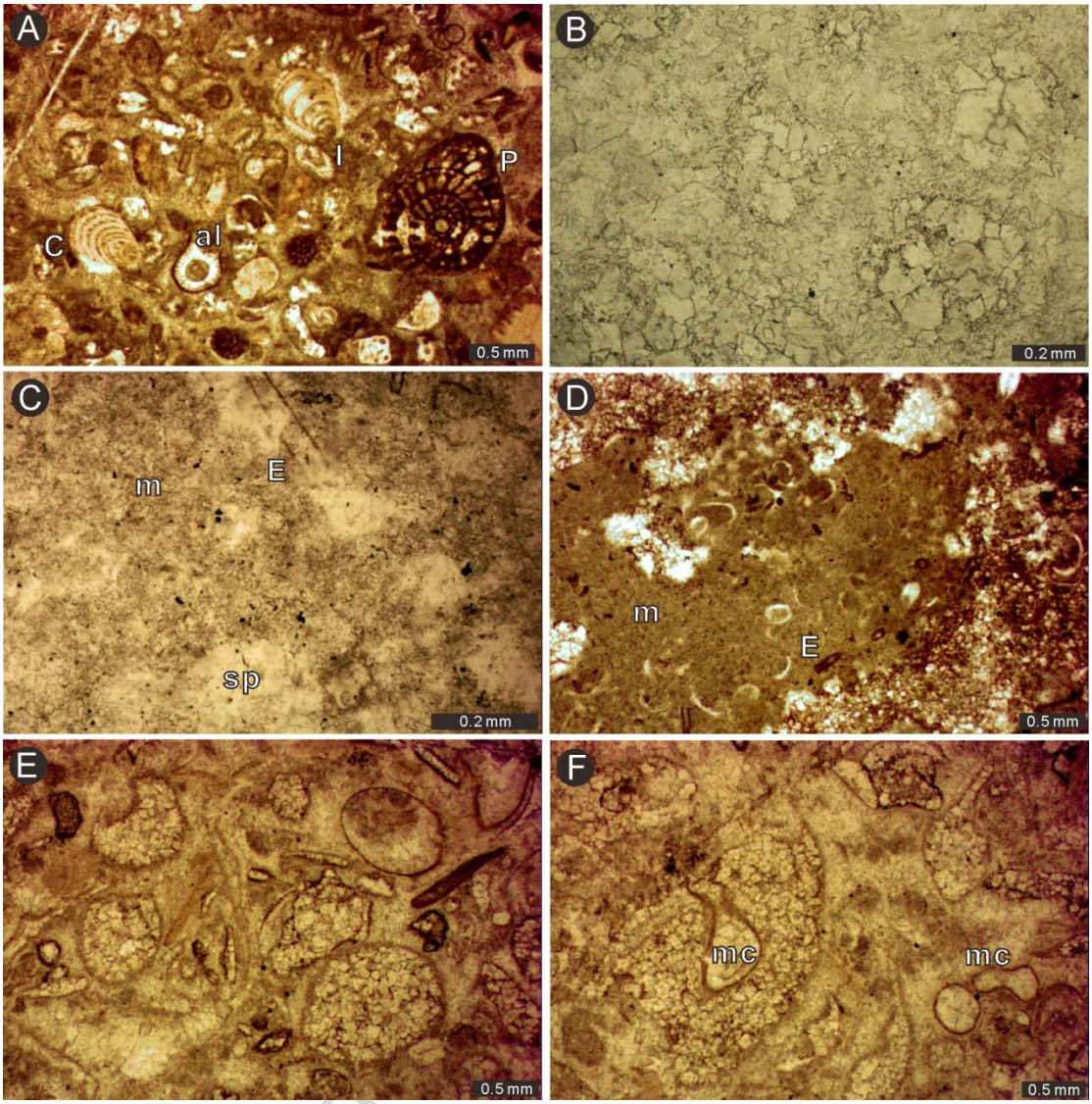

Figure 4

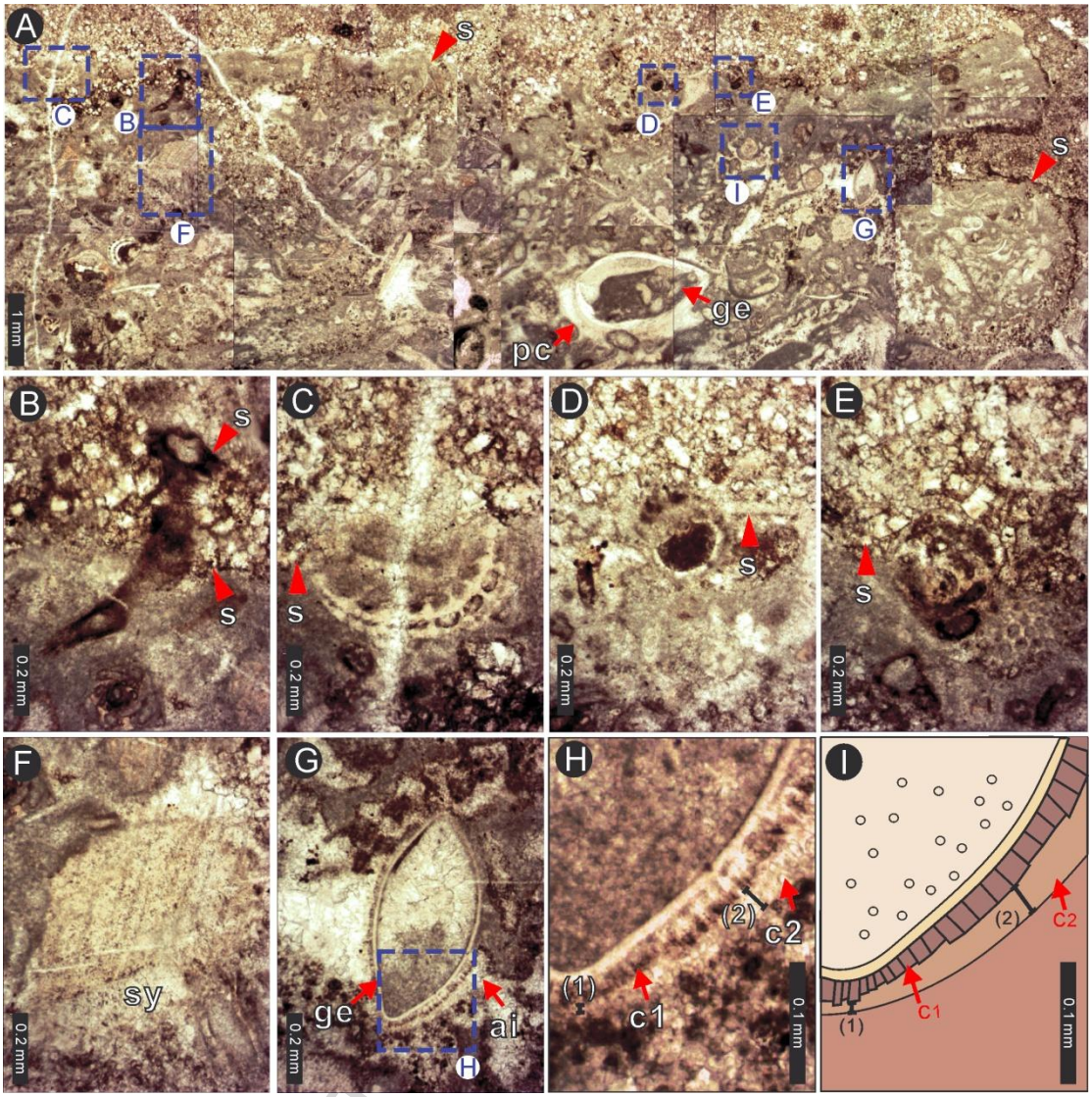

Figure 5

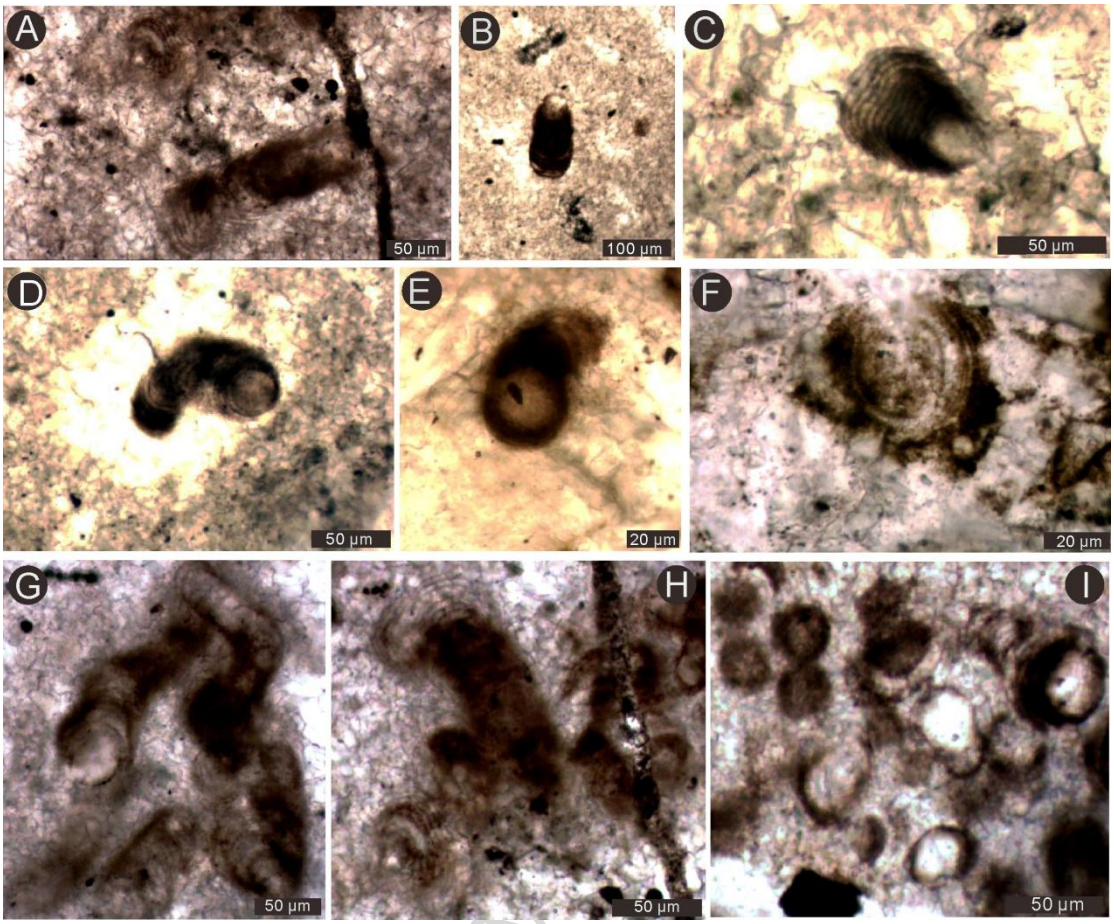

Figure 6

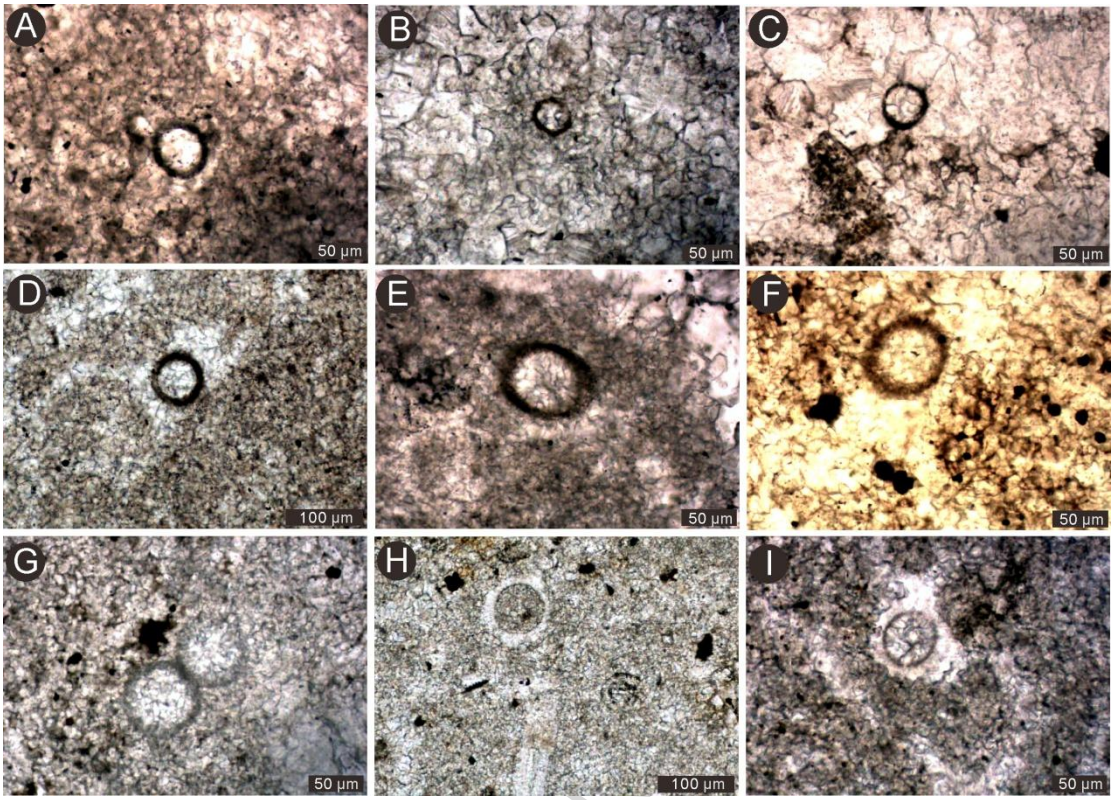

Figure 7

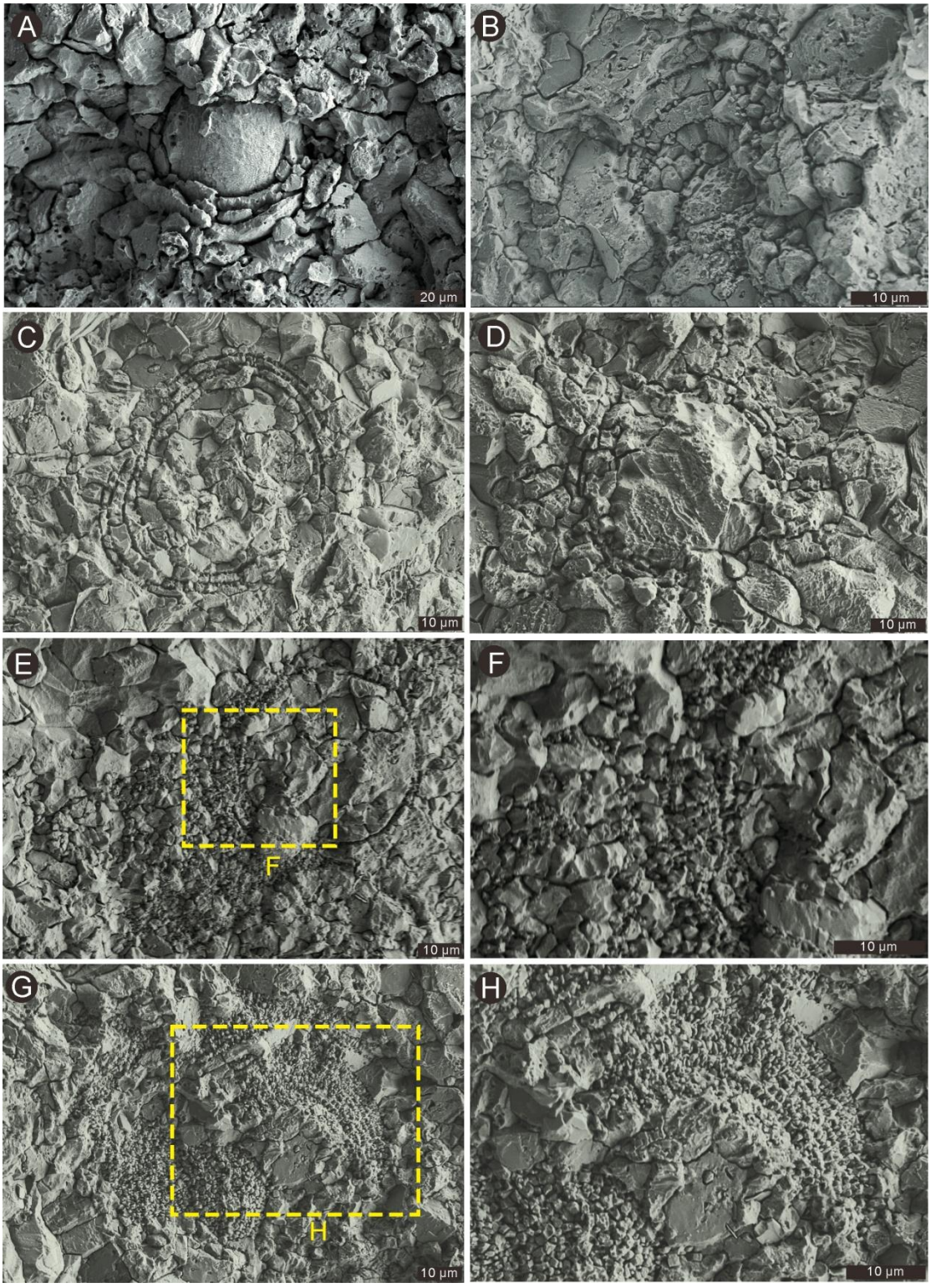

Figure 8

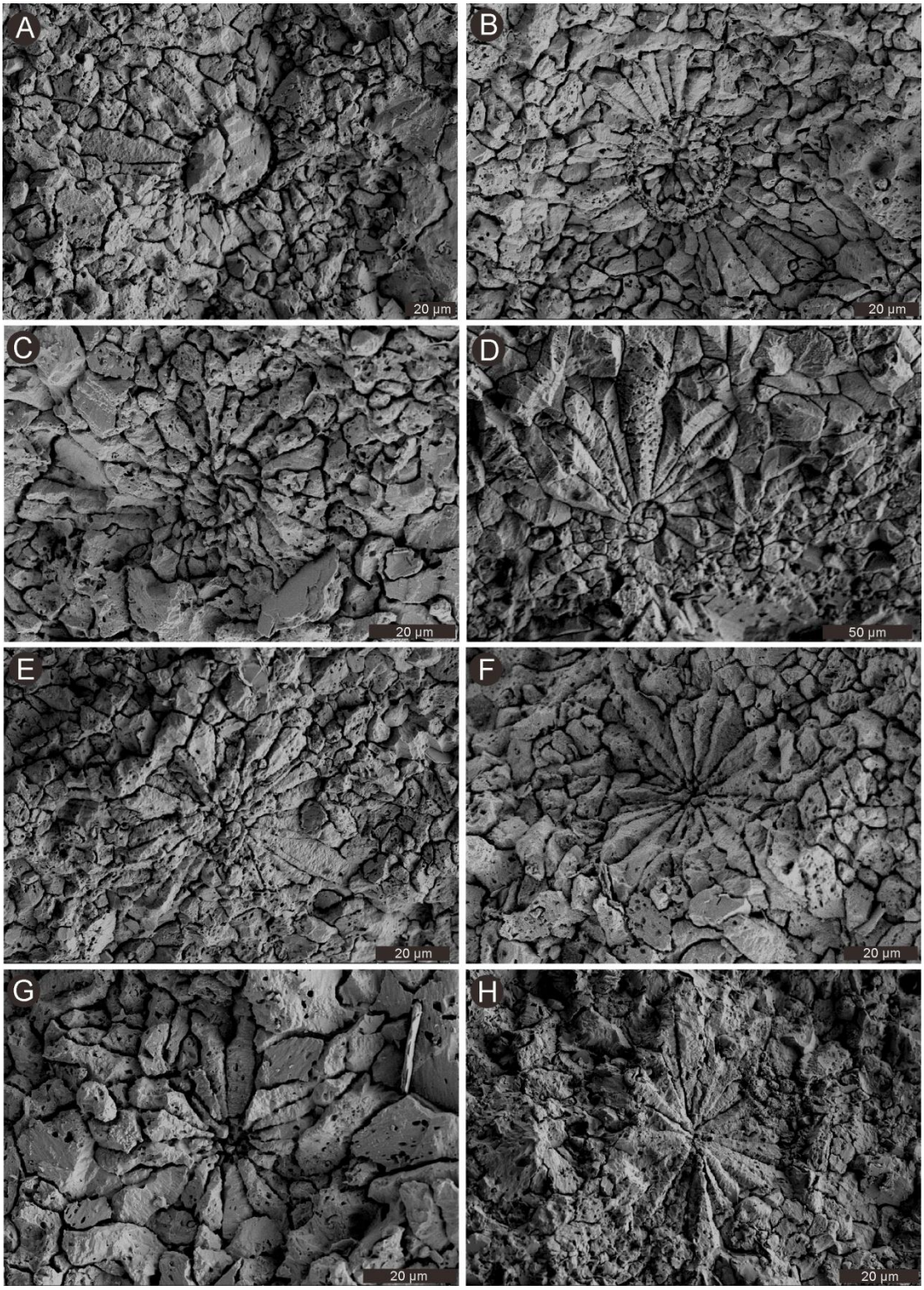

Figure 9

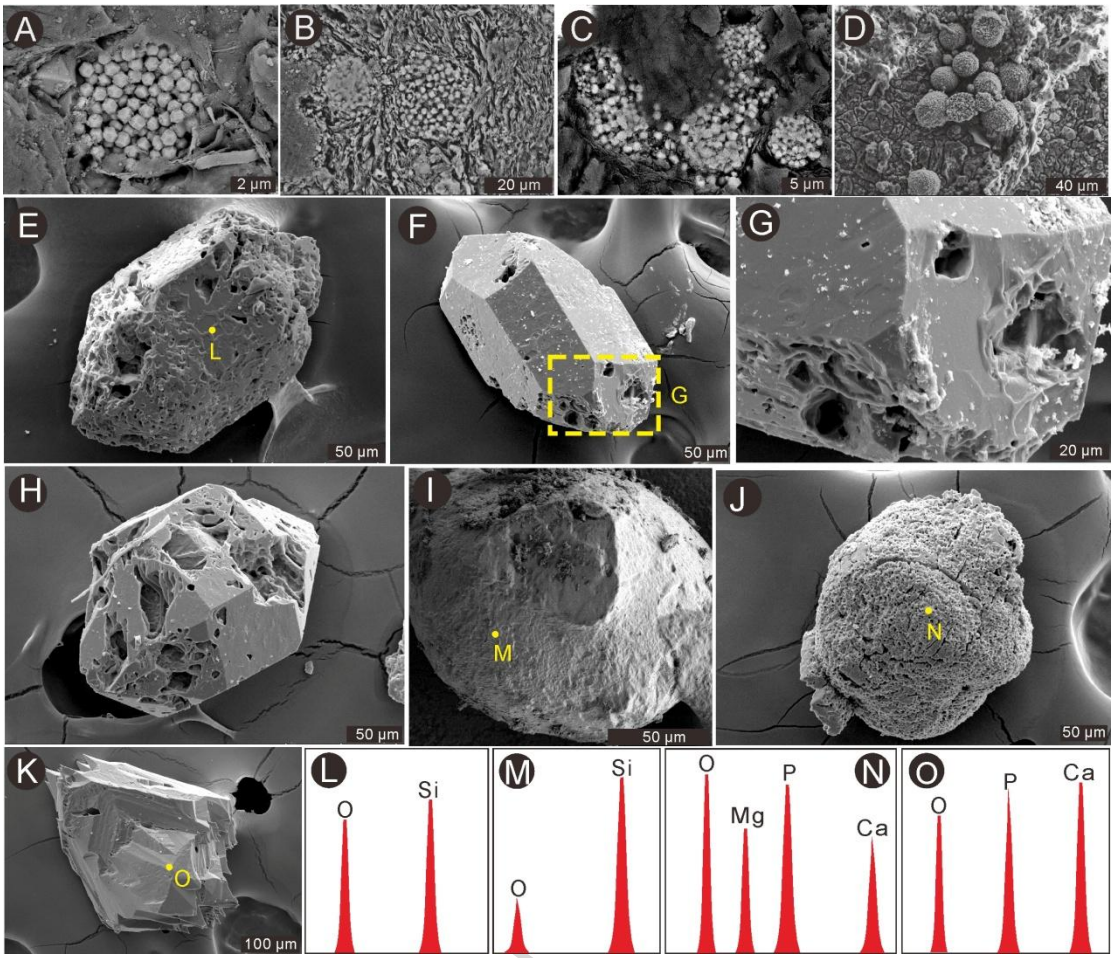

Figure 10

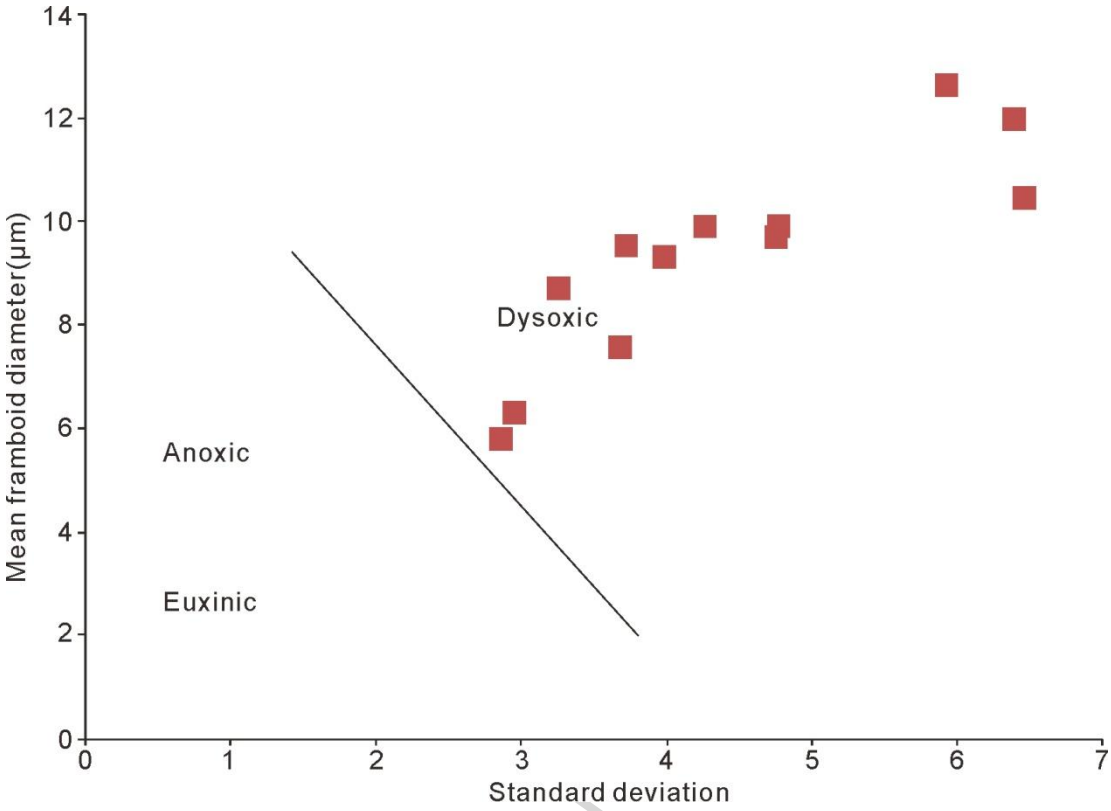

Figure 11

Highlights:

(1) “Gakhumella”, coccoid-like spheroids, bacterial clump-like spheroids, and hollow spheroids probably have played an important role in accretion of the microbialites in this site;

(2) Pyrite framboid size and morphology show that the microbialite may have been deposited in lower to upper dysoxic conditions.

(3) Microbial bloom, indicated by the widespread PTBMs seems not to be linked with the contemporaneous volcanism.